AER/AGS Special Report 130

Alberta Energy Regulator

Estimating the Curie Point Depth Isotherm in Alberta Using Aeromagnetic Data

AGS
ALBERTA GEOLOGICAL SURVEY

AER/AGS Special Report 130

Estimating the Curie Point Depth Isotherm in Alberta Using Aeromagnetic Data

H.H. Hassan[1] and P. Harms[2, 3]

[1] Multiphysics Imaging Technology
[2] 4th Resource Corp.
[3] GEOSEIS Inc.

March 2026

ISBN 978-1-4601-5745-9

Hassan, H.H. and Harms, P. (2026): Estimating the Curie point depth isotherm in Alberta using aeromagnetic data; Alberta Energy Regulator / Alberta Geological Survey, AER/AGS Special Report 130, 54 p.

Author addresses:

H.H. Hassan
Multiphysics Imaging Technology
506, 683 10 Street SW
Calgary, AB T2P 5G3
Canada

Tel: 403.714.9798
Email: hassan.hassan@multiphysics.ca

P. Harms
4th Resource Corp.
520, 727 7 Avenue SW
Calgary, AB T2P 0Z5
Canada

Tel: 403.608.1560
Email: phil.harms@4thresource.ca

P. Harms
GEOSEIS Inc.
1605 4A Street NW
Calgary, AB T2M 3B3
Canada

Tel: 403.608.1560
Email: pharms@geoseis.ca

Published March 2026 by:
Alberta Energy Regulator
Alberta Geological Survey
Suite 205
4999 – 98 Avenue NW
Edmonton, AB T6B 2X3
Canada

Tel: 780.638.4491

Email: AGS-Info@aer.ca
Website: ags.aer.ca/

Contents

Appendices

Digital Appendix 1 – Merged gravity magnetic data
The appendix is in the accompanying folder entitled ‘MERGED_gravity_magnetic_data’, located in the download zip file.

Digital Appendix 2 – Moho from 3D gravity inversion
The appendix is in the accompanying folder entitled ‘MOHO-from_3D_gravity_inversion’, located in the download zip file.

Digital Appendix 3 – Results of centroid method
The appendix is in the accompanying folder entitled ‘RESULTS_Centroid_method’, located in the download zip file.

Digital Appendix 4 – Results of fractal method
The appendix is in the accompanying folder entitled ‘RESULTS_Fractal_method’, located in the download zip file.

Foreword

The Alberta Geological Survey (AGS) contracted Multiphysics Imaging Technology, 4th Resource Corp., and GEOSEIS Inc. to estimate the Curie point depth (CPD) isotherm across Alberta using aeromagnetic data. The CPD represents the depth at which crustal rocks reach approximately 580°C, the temperature at which ferromagnetic minerals lose their magnetization. Mapping this thermal boundary provides a regional proxy for crustal heat distribution, geothermal gradients, and mantle-derived heat flow, supporting geothermal resource evaluation and tectonic studies.

Residual magnetic intensity (RMI) grids were compiled from high-resolution airborne magnetic surveys acquired by the AGS (2021–2024), and supplemented with lower-resolution datasets from the Geological Survey of Canada and the U.S. Geological Survey. The RMI grid was subdivided into 660 overlapping 160 by 160 km windows, spaced at 40 by 40 km intervals between centroids. Of these, 417 windows fall within Alberta, providing dense spatial sampling for spectral analysis. Fast Fourier transform (FFT) power-spectrum analysis was applied to each window, and CPD was estimated using both centroid and fractal spectral methods. The results were interpolated to produce a continuous provincial grid.

The CPD estimates range from approximately 8 to 30 km, with a mean depth of 23 ±4 km. Shallow CPD values occur beneath the Rocky Mountain fold-and-thrust belt, whereas deeper values characterize the Rae and Hearne cratons. Intermediate depths are observed along the Snowbird tectonic zone. From these CPD results, geothermal gradients (average of 26 ±5°C/km) and heat-flow values (48 to 149 mW/m²) were derived, indicating elevated thermal conditions in southwestern Alberta. These estimates are consistent with borehole-based measurements and global heat-flow compilations, though they exclude radiogenic heat contributions from granitic rocks.

A complementary three-dimensional (3D) inversion of Bouguer gravity data was conducted to estimate Mohorovičić discontinuity (Moho) depths, which range from 35 to 46 km. A moderate negative correlation ($r \approx -0.70$) between CPD and Moho depth suggests that thicker crustal regions may retain heat due to low thermal conductivity, resulting in shallower thermal isotherms above a deeper lithosphere.

This work was completed under the Mineral Grant provided by the Government of Alberta dated June 22, 2021.

Estimating Curie Point Depth (CPD) isotherm in Alberta using aeromagnetic data

By:

Hassan H. Hassan[1],

Phil Harms[2,3]

1. Multiphysics Imaging Technology
2. 4th Resource Corporation
3. GEOSEIS Inc.

March 2025

All work performed and information provided is of the highest technical quality possible given data limitations and uncertainties at the time the work was completed. Conclusions and recommendations are made from the interpretation of all data available to GEOSEIS at the time of the study and represent our current understandings based on the data and our professional experience. GEOSEIS reserves the right to modify and update conclusions and recommendations with the advent of new data, technology, operational results, experience or ideas. GEOSEIS has done its best to ensure the accuracy and integrity of the data and bears no responsibility for incorrect conclusions drawn from problematic data.

Any reports or work products must be viewed holistically, and conclusions and recommendations must be observed within the context of the wider body of work including all supporting information, documented assumptions, limitations of the data as well as any corresponding files or presentations in the report, previous reports and referenced documents. GEOSEIS bears no responsibility for any selective and out-of-context representations of the work and resulting conclusions or decisions.

The authors of, and contributors to, this report make no guarantees to the predictability of, economic valuation of associated assets, risks to, or consequences of, the material in the report. As with all interpretative work, there is a certain measure of subjectivity and uncertainty in approach and conclusions. GEOSEIS has done its best to make reasonable assumptions and document assumptions, unknowns and uncertainties.

This report contains conclusions drawn from and representations of licensed and proprietary data owned or licensed by the client. Any use or disclosure outside of the intended audience should seek permission and/or clarification of data ownership and viewing limitations from the client and authors of this report.

<table>
<tr><th colspan="2">AUTHORS & APPROVERS</th><th colspan="3">AUTHENTICATION</th></tr>
<tr><td>Authors:</td><td>Hassan H. Hassan,
Multiphysics Imaging Technology

Phil Harms, P. Geo,
4th Resource Corp., GEOSEIS Inc.</td><td colspan="3">February 19, 2026</td></tr>
<tr><td rowspan="5">Peer Review:</td><td rowspan="5">Dan Kalmanovitch, P. Eng,
4th Resource Corp, GEOSEIS Inc.

Arif Rabbani, PhD, P. Geo,
Alberta Geological Survey

David Birnie, P. Geo,
GEOSEIS Inc.</td><td colspan="3">VALIDATION</td></tr>
<tr><td>PERMIT TO PRACTICE:</td><td colspan="2">GEOSEIS Inc.</td></tr>
<tr><td>RM SIGNATURE:</td><td colspan="2"></td></tr>
<tr><td>RM APEGA #:</td><td colspan="2">24419</td></tr>
<tr><td>DATE:</td><td colspan="2">Feb. 9, 2026</td></tr>
<tr><td>Client:</td><td>Arif Rabbani, PhD, P. Geo,
AGS / AER</td><td>PERMIT NUMBER:</td><td colspan="2">P-8794</td></tr>
<tr><td colspan="3"></td><td colspan="2">The Association of Professional Engineers and Geoscientists of Alberta (APEGA)</td></tr>
<tr><th>VERSION</th><th>DATE</th><th>AUTHORS</th><th colspan="2">DESCRIPTION / CHANGES</th></tr>
<tr><td>1.0</td><td>March 31, 2025</td><td>H. Hassan,
P. Harms</td><td colspan="2">Final Report</td></tr>
<tr><td>1.1</td><td>February 6, 2026</td><td>A. Rabbani
M. Grobe</td><td colspan="2">Minor text edits</td></tr>
<tr><td>1.2</td><td>February 19, 2026</td><td>A. Rabbani,
P. Harms</td><td colspan="2">Minor text edits and formatting</td></tr>
</table>

SUMMARY

With increasing demands for alternative and renewable energy, geothermal energy is emerging as a viable source. In 2021, the Alberta Geological Survey (AGS) and Alberta Energy Regulator (AER) initiated the Mineral and Geothermal Mapping Programs, as part of the Government of Alberta's Mineral Strategy and Action Plan (Alberta Energy, 2021). The primary objective is to enhance the availability of public geoscience information on Alberta's mineral, geothermal, and other emerging resources.

This study is one of the projects supported by the program and is designed to estimate the Curie Point Depth (CPD) isotherm using the radial average power spectrum of magnetic data across Alberta. CPD is a widely used regional-scale geothermal analysis tool to assess crustal rock temperatures. Reports suggest that shallow CPD isotherms often coincide with potential geothermal resource areas. Additionally, the CPD isotherm is a valuable tool for studying the tectonic and thermal evolution of the lithosphere.

The concept of using the power spectrum of magnetic data to estimate CPD is not new. It was introduced in the 1970s as a reconnaissance tool for geothermal exploration in Japan. However, due to the increasing demand for clean, renewable, and environmentally sustainable energy sources, this technique has garnered significant attention in recent years.

The CPD represents an isotherm surface formed deep in the Earth’s crust, where crustal rock temperatures reach the Curie point of 580°C. At this temperature, ferromagnetic minerals, such as magnetite (Fe_3O_4), lose their magnetic properties and become non-magnetic. Consequently, the CPD corresponds roughly to the Depth to the Bottom of Magnetic Sources (DBMS) where magnetization diminishes to zero. By analyzing magnetic data, we can map the maximum depths detectable, as DBMS is considered equivalent to CPD depth.

The radial power spectrum of magnetic data is a widely used method to estimate the depth of magnetic layers within the Earth's crust. Magnetic signals measured at the Earth's surface combine signals from sources at various depths. Shallow sources near the surface are associated with high-frequency, short-wavelength magnetic anomalies, whereas deeper sources correspond to low-frequency, long-wavelength anomalies. The Fast Fourier Transform (FFT)-based power spectrum, which displays the complete frequency range of a signal, is an ideal tool for estimating average depths of magnetic sources in the crust.

Various approaches exist for estimating CPD from the power spectrum of magnetic data. In this study, we used two of the most popular methods: the "centroid" and "fractal" approaches. The CPD results were then used to approximate the "CPD derived" average geothermal gradient ($\Delta T/\Delta Z$) and heat flow (Q) for the study area. The CPD derived geothermal indicators do not factor in shallow variability and are designed to be indicative of mantle derived geothermal trends.

To explore potential correlations between the Moho surface and the computed CPD isotherm, we performed a 3D gravity structural inversion on Alberta's Bouguer gravity grid using the Parker-Oldenburg algorithm to estimate the Moho depth.

The magnetic data for this study were obtained from multiple datasets. The primary dataset, obtained from the Alberta Geological Survey (AGS), is a composite of several high-resolution aeromagnetic (HRAM) surveys, including the most recent HRAM data covering specific areas in Alberta. This dataset provides comprehensive coverage of Alberta, except for the Rocky Mountain region. To fill gaps and extend coverage near Alberta's borders, we incorporated low-resolution, publicly available aeromagnetic data from the Geological Survey of Canada (GSC) and Montana.

The CPD isotherm across the study area was derived from the residual magnetic intensity (RMI) grid, corrected for the International Geomagnetic Reference Field (IGRF). The RMI grid was divided into 660 overlapping blocks, each measuring 160 × 160 km. Among these, 417 blocks are located within Alberta. This block size effectively captures long-

wavelength magnetic signals essential for DBMS calculations. Fast Fourier Transform (FFT) was applied to each block to generate power spectrum plots, from which DBMS was computed using the centroid and the fractal methods. The CPD values at the block centers were then gridded using the minimum curvature technique for further processing and interpretation.

The estimated average CPD in Alberta, derived from both methods, is 23.4 ± 3.5 km, with observed values ranging from 8.1 to 30.5 km. The results from both approaches show a notable similarity.

Regionally, CPD depths vary significantly across Alberta. In southwestern Alberta, particularly beneath the Rocky Mountain Belt, CPD depths are relatively shallow (~15 km). In contrast, deeper CPD values are observed in the Interior Plains (~25 km beneath the Rae Craton and ~27 km under the southeastern Hearne Craton). The Snowbird Tectonic Zone (SBTZ), located at the boundary between the Alberta Basin and the Hearne Craton, shows intermediate CPD depths (~20 km).

Additionally, geothermal gradients and heat flow values were derived from CPD data. Heat flow values in Alberta range between 47.7 and 148.9 mW/m², aligning well with existing regional heat flow data. However, these calculations do not account for radiogenic heat generated by uranium, thorium, and potassium within granitic rocks of the Precambrian crystalline basement underlying the Western Canada Sedimentary Basin. The observed shallowing of the CPD isotherm surface beneath the Rocky Mountain Belt is consistent with previous studies and may be attributed to multiple thermal and geological processes, including elevated radiogenic heat, a hotter mantle, small-scale heat convection, and lithosphere delamination.

A 3D inversion of Bouguer gravity anomalies across the study area indicates that the Moho depth ranges from 35 km to 46 km, with an average of 38.3 ± 2.2 km below sea level. Statistical analysis reveals a moderate negative correlation coefficient (r = ~ -0.70) between the inverted Moho surface and the computed CPD isotherm.

The observed negative correlation may stem from crustal rocks with low thermal conductivity retaining heat. This process leads to a shallow CPD while sustaining a deep Moho. Such patterns are commonly seen in ancient cratons, like the Canadian Shield, where the thick crust results in a deep Moho. Meanwhile, the low thermal conductivity of these rocks traps heat, contributing to a shallow CPD.

The contrasting characteristics of the Moho and CPD boundaries likely explains this relationship. The Moho represents a lithological boundary, marking compositional changes in the Earth's crust and mantle, while the CPD reflects a thermal boundary, indicating the depth at which temperatures reach the Curie point.

INTRODUCTION

Study Background and Objectives

Geothermal energy refers to the natural heat stored beneath the Earth's surface. It can be released as steam or hot water, or accessed by drilling deep wells to harness the energy for thermal applications or electricity generation.

Geophysical techniques, particularly gravity and magnetic methods, whether applied independently or in combination, play a crucial role in geothermal exploration. These methods help identify igneous rocks that may serve as heat sources at various depths within the Earth's crust. Additionally, gravity and magnetic techniques are effective in mapping faults and fractures, which act as conduits for geothermal fluids, allowing them to migrate from deeper crustal layers to the surface.

Magnetic data, in particular, has an additional advantage over other geophysical techniques as a reconnaissance tool for mapping the Curie Point Depth (CPD) isotherm surface. At the CPD isotherm (580°C), crustal rocks lose their magnetic properties, causing the CPD isotherm surface to align with the Depth to the Bottom of Magnetic

Sources (DBMS). Therefore, the DBMS computed from magnetic data represents the CPD isotherm surface (Ravat *et al*., 2007).

The objective of this study is to compute the DBMS using magnetic data and subsequently infer the CPD isotherm of the study area.

The geothermal regime in Alberta is dominated by sedimentary basin processes. The two main types of heat transport are heat which flows upward from the mantle and heat which is generated within the crust from the decay of radioactive elements (Bachu and Burwash, 1994) in both sedimentary and crystalline basement rocks. Shallow geological variability results in local variation in convective and conductive heat transfer mechanisms. Localized heat flow and geothermal gradient anomalies result.

Heat flow from the mantle has a steady state component deep from the interior of the earth (Bachu and Burwash, 1994). CPD variability is assumed to be proportional to mantle generated heat sources and is represented by the 580^{o}C isotherm. The CPD measures the base of magnetic sources and therefore takes no consideration for localized and shallow variability in the heat flow regime. Therefore, the CPD measures a background gradient where significant higher frequency variation is expected.

Building on the work presented at the 2024 GeoConvention in Calgary, Alberta (Hassan and Harms, 2024a), the CPD analysis has been expanded to cover the entire province of Alberta shown in Figure 1. The expansion of this work is in collaboration with the Alberta Geological Survey (AGS) and is paid for by the Alberta Minerals Grant as part of the Government of Alberta's Minerals Strategy and Action Plan (Alberta Energy, 2021). This plan seeks to increase the availability of public geoscience information on Alberta's emerging resources. As part of this program, between 2021 and 2024 the AGS acquired modern high-quality airborne magnetic data over the entire province outside the mountains and foothills, and localized gravity data, filling data gaps and replacing outdated data (Alberta Geological Survey, 2024). All data and publications from this program are freely available on the AGS Mineral Mapping program webpage (Alberta Geological Survey, 2025).

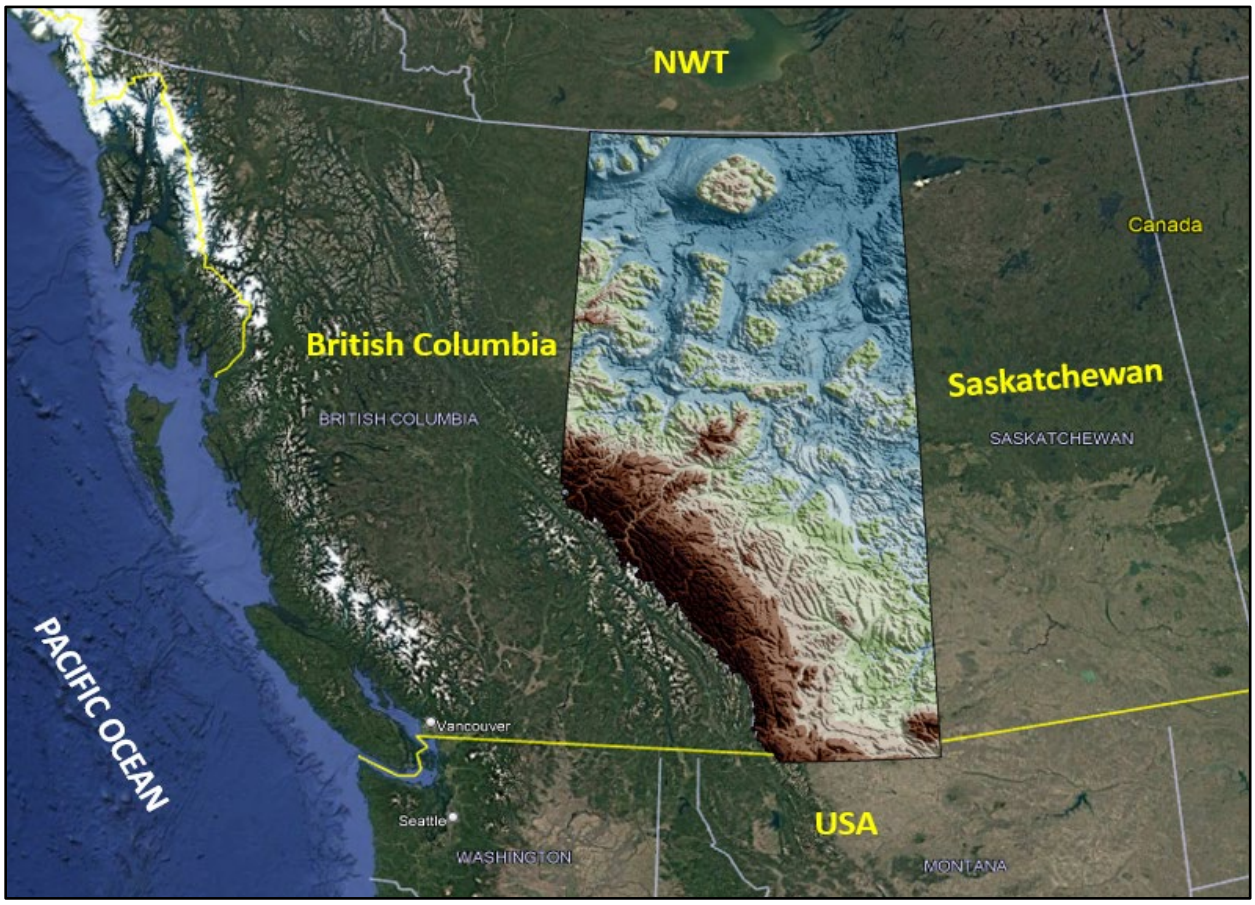

Figure 1. Index map showing NASA SRTM topography of the study area overlain on a Google Earth base image.

GEOLOGICAL SETTING

Alberta's geological history spans billions of years and encompasses diverse tectonic activities, resulting in two distinct geological settings:

1. **The Rocky Mountain Belt** to the west

2. **The Interior Plains** to the east of the Rocky Mountain Belt

The Rocky Mountain Belt

Formed during the Late Cretaceous to Early Tertiary periods, the Rocky Mountain Belt (Figure 2) originated from the collision of the North American and Pacific Plates during the Cordilleran orogeny (Porter *et al.*, 1982). This tectonic activity caused the sedimentary rocks to fold, fault, and uplift, creating mountainous terrains. These sedimentary rocks consist predominantly of limestone, sandstone, and shale, deposited in shallow marine environments during the Paleozoic and Mesozoic eras. The Rocky Mountain Belt exhibits significant deformation, dominated by thrust faults (low-angle reverse faults) and synclinal and anticlinal structures.

The Interior Plains

The Interior Plains, characterized by relatively flat terrain, are primarily underlain by the Western Canada Sedimentary Basin (WCSB), which covers over 95% of Alberta (Majorowicz *et al*., 2014). The WCSB is a thick wedge of sedimentary rocks that extends from the Canadian Shield in northeastern Alberta to the Rocky Mountain Belt in the west (Porter *et al.*, 1982). The thickness of the sedimentary rocks increases from zero in northeast Alberta to over 7 km towards the west. These rocks, formed during the Paleozoic, Mesozoic, and Cenozoic eras, host significant petroleum, natural gas, and coal resources, making Alberta a key player in the energy sector. These Phanerozoic sedimentary rocks overlie Precambrian and Archean crystalline basement rocks, which primarily consist of metasedimentary rocks and felsic igneous rocks such as granite and rhyolite (Burwash and Power, 1991). Granite and rhyolite are typically rich in uranium, thorium, and potassium, making them potential sources of radiogenic heat within the Earth's crust. Previous research by the Geological Survey of Canada identified a significant warm-water reservoir (~ 60°C) within the WCSB, located near the contact between the Precambrian basement and overlying sedimentary rocks, at a depth of ~2.2 km (Jessop, 1998).

Over time, tectonic and metamorphic processes during the Archean and Proterozoic periods reactivated pre-existing faults and shear zones within the basement, propagating upward to form various fault systems in the overlying sedimentary rocks. These include reverse faults in the foreland thrust belt, normal faults within the basin, and NE-SW trending strike-slip faults along major tectonic boundaries, such as the Great Slave Lake Shear Zone, Peace River Arch, and the Snowbird Tectonic Zone (Figure 2).

Lithotectonic Domains of the Precambrian Basement

Using gravity and magnetic data, researchers have divided the Precambrian basement into several lithotectonic domains (Ross *et al*., 1994; Pilkington *et al*., 2000). These domains are periodically updated as new data emerges. The most recent classification by Pilkington *et al*. (2000), shown in Figure 3, identifies the following groups based on magnetic signatures:

1. **Domains with weak magnetic anomalies (Hottah, Chinchaga, and Thorsby):** Characterized by low-amplitude magnetic anomalies, likely caused by silicate-rich rocks with low magnetic susceptibility (paramagnetic minerals).

2. **Domains with moderate magnetic anomalies (Wabamun, Lacombe, Rimbey, Loverna, and Medicine Hat):** Associated with moderate-amplitude magnetic anomalies, likely resulting from ferrimagnetic minerals (e.g., magnetite) within mafic and granitoid igneous rocks.

3. **Domains with strong magnetic anomalies (Buffalo High, Buffalo Utikuma, Talston, Ksituan, and Matzhiwin):** Exhibiting the largest magnetic anomalies, caused by intermediate igneous rocks formed in magmatic arc environments.

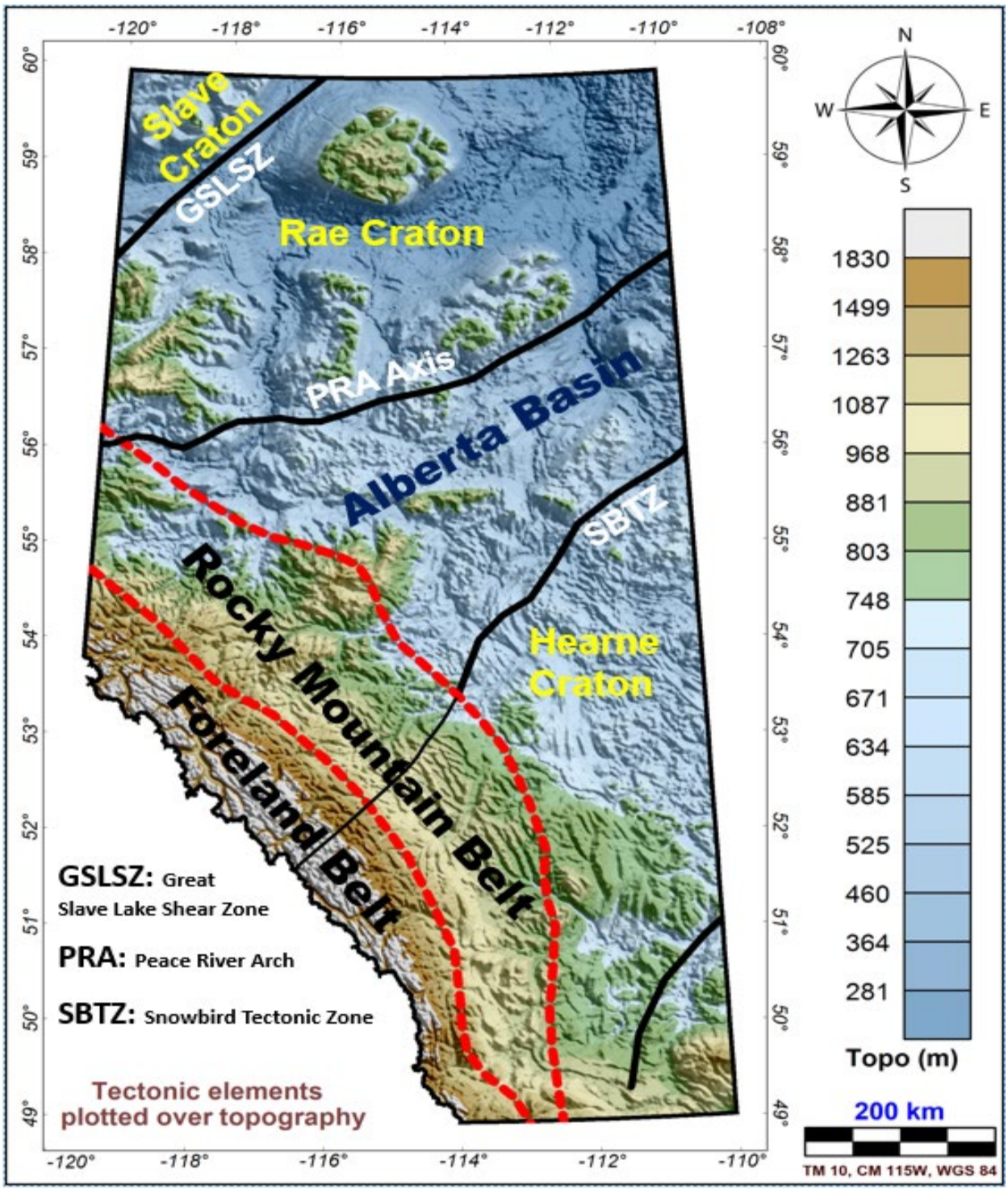

Figure 2. Tectonic elements (Pilkington et al., 2000) overlain on NASA SRTM topography across the study area.

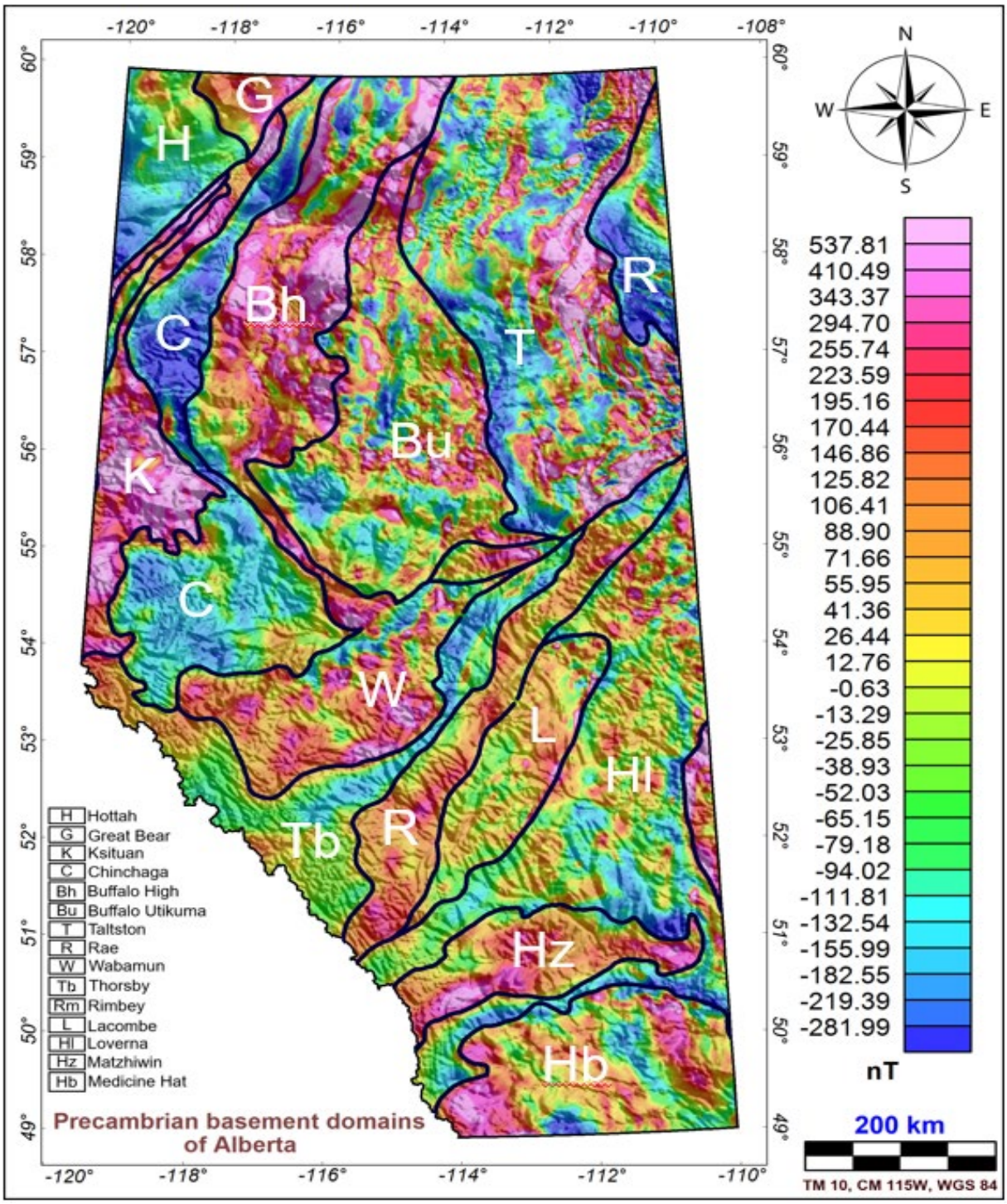

Figure 3. Precambrian lithotectonic domains (Pilkington et al., 2000) overlain on residual magnetic intensity (RMI).

GEOPHYSICAL DATA SOURCES

The composite magnetic grid (Figure 4) used to calculate the CPD isotherm in this study was derived from multiple sources. The primary data source was the recently acquired aeromagnetic dataset provided by the AGS. AGS recently released a high-quality composite aeromagnetic grid (Figure 5), created by integrating data from several high-resolution aeromagnetic (HRAM) surveys.

The data for this composite grid included newly acquired HRAM surveys conducted by EON Geosciences between 2021 and 2024, as well as older HRAM datasets purchased from CHAD Data Ltd. (formerly GEDCO). These HRAM surveys were conducted with flight line spacing ranging from 400 to 800 meters, tie line spacing ranging from 1,200 to 2,500 meters, and low-altitude terrain clearance between 120 and 200 meters. This dataset provides comprehensive coverage across Alberta, except for the Rocky Mountain region.

To address gaps over the Rocky Mountain region and extend data coverage near Alberta's borders, low-resolution, publicly available aeromagnetic datasets from the Natural Resources Canada (Natural Resources Canada 2025a) and the US Geological Survey (McCafferty et al., 1998) were merged with the AGS high-resolution aeromagnetic data. The resulting merged aeromagnetic grid is presented in Figure 4. The CPD isotherm across Alberta was computed using the Residual Magnetic Intensity (RMI) grid, which was corrected for the International Geomagnetic Reference Field (IGRF).

The Bouguer gravity data (Figure 6), with a spatial resolution of 2 kilometers, was obtained from a public geophysical database available on the Natural Resources Canada website. (Natural Resources Canada 2025b). In the southern region, these data were merged with publicly available Bouguer gravity datasets from the US Geological Survey (McCafferty *et al*., 1998).

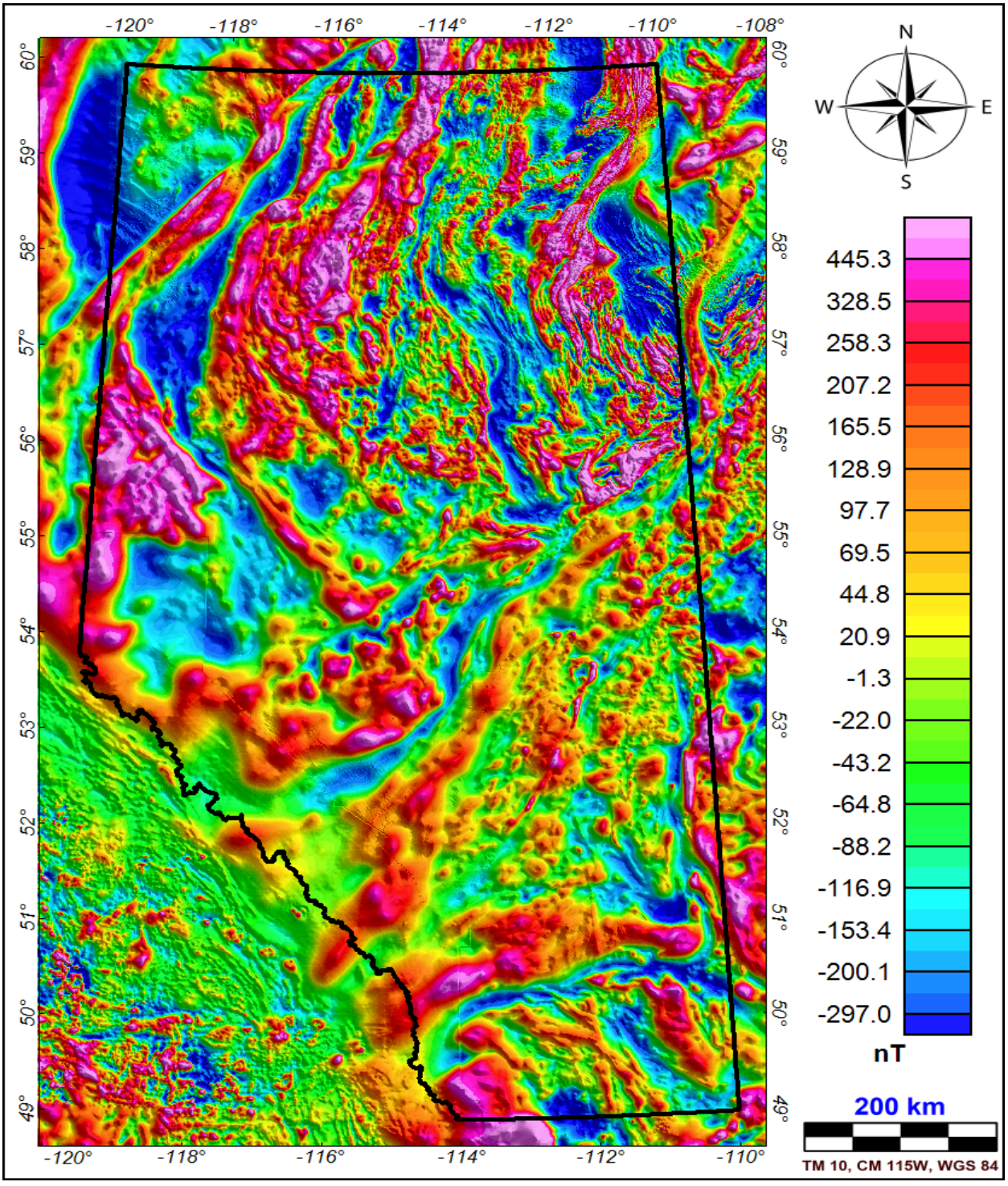

Figure 4. Merged residual magnetic intensity (RMI) grid for Alberta compiled from three sources: Alberta Geological Survey (2024), Natural Resources Canada (2025a), and McCafferty et al. (1998).

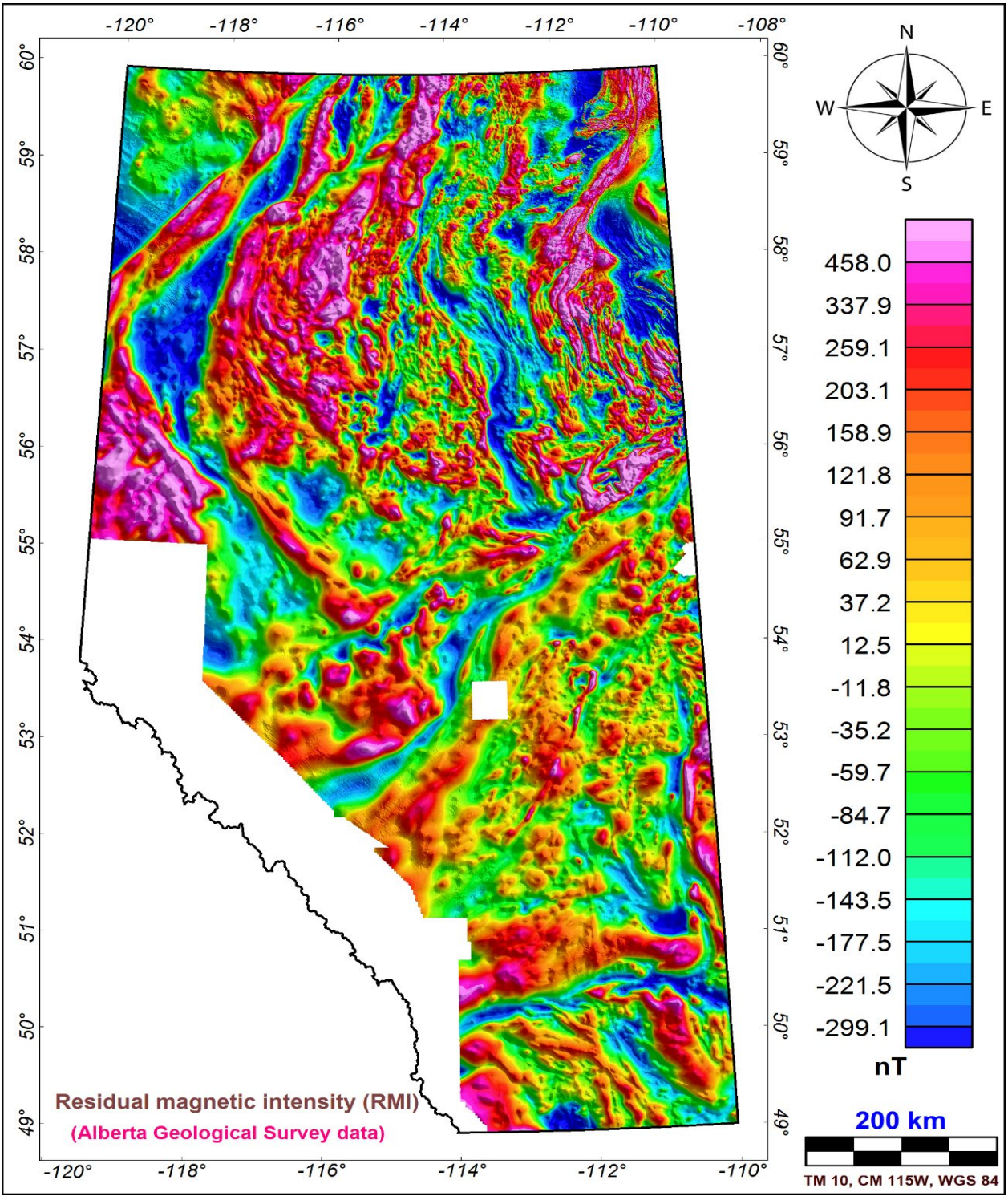

Figure 5. AGS merged (RMI) aeromagnetic data from recent AGS surveys (Alberta Geological Survey, 2024).

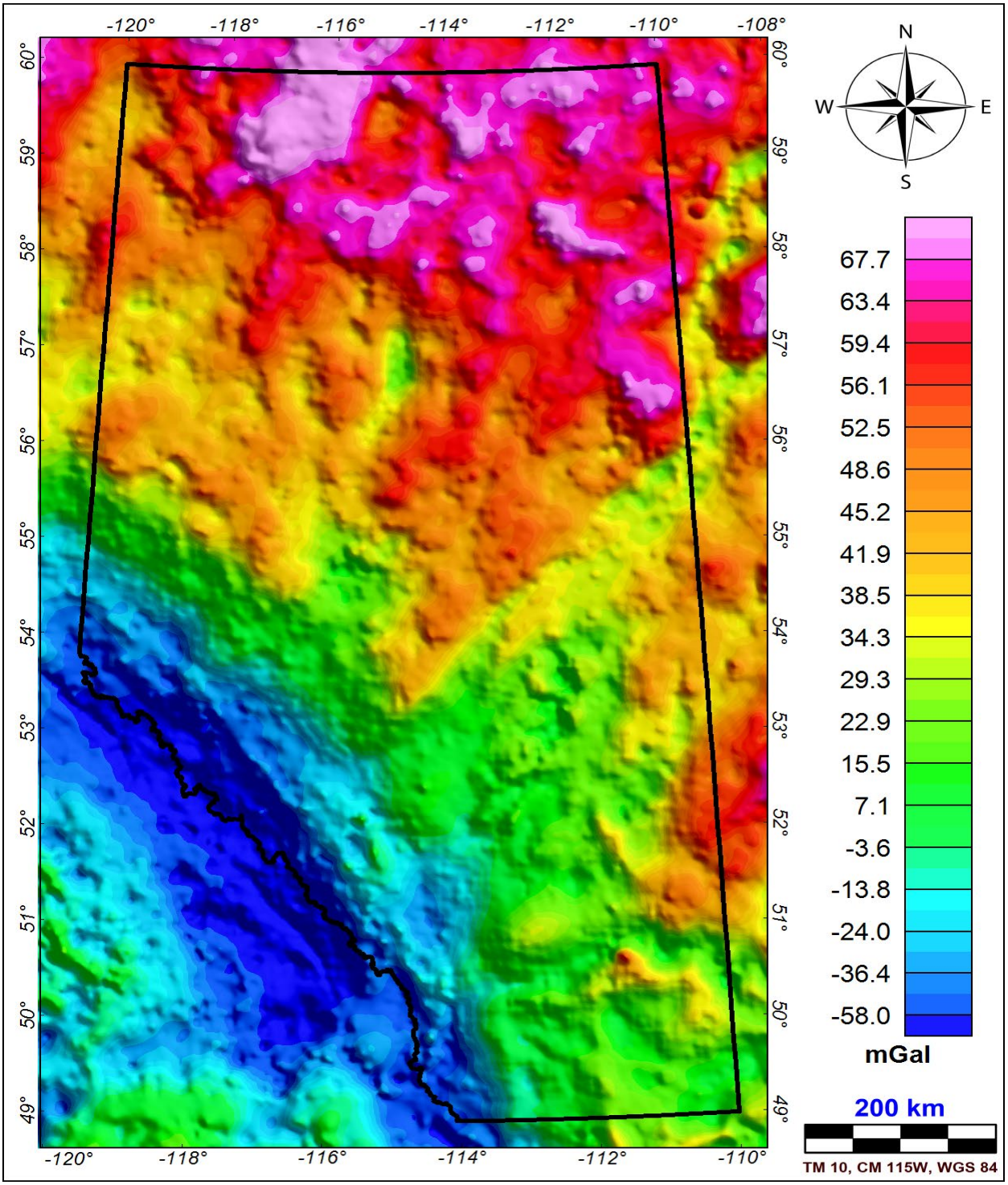

Figure 6. Merged Bouguer gravity grid (Natural Resources Canada, 2025b).

The final merged aeromagnetic (Figure 4) and gravity (Figure 6) datasets for the study area use the following projection parameters:

Data Projection

- **Projection:** Alberta 10 TM
- **Datum:** NAD83 (WGS84)
- Central Meridian: 115° West
- **False Easting:** 500,000 meters
- False Northing: 0 meters
- Scale Factor: 0.9992

METHODOLOGY

To estimate the CPD, the RMI grid shown in Figure 4 was divided into 660 overlapping blocks, each measuring 160 x 160 km (Figure 7), of which 417 fall within Alberta. The resulting CPD grid is spaced 40 x 40 km to the centroid of each block. This block size was selected after testing various window sizes in a prior study by the authors (Hassan and Harms, 2024a). The chosen size effectively captures long-wavelength signals essential for CPD computation, as it exceeds five times the maximum CPD in the study area (~30 km). Blakely (1988) recommended that block size should be approximately five times the anticipated CPD.

Several methods exist for estimating CPD from magnetic data. Among these, the Fast Fourier Transform (FFT) based radially averaged power spectrum method remains the most widely used (Figure 8). Originally introduced by Spector and Grant (1970) to estimate the depth to crystalline basement rocks in sedimentary basins, this method has undergone modifications and is now extensively applied to calculate DBMS as a proxy for the CPD isotherm surface (e.g., Bhattacharyya and Leu, 1975, 1977; Bouligand *et al*., 2009; Li *et al*., 2010).

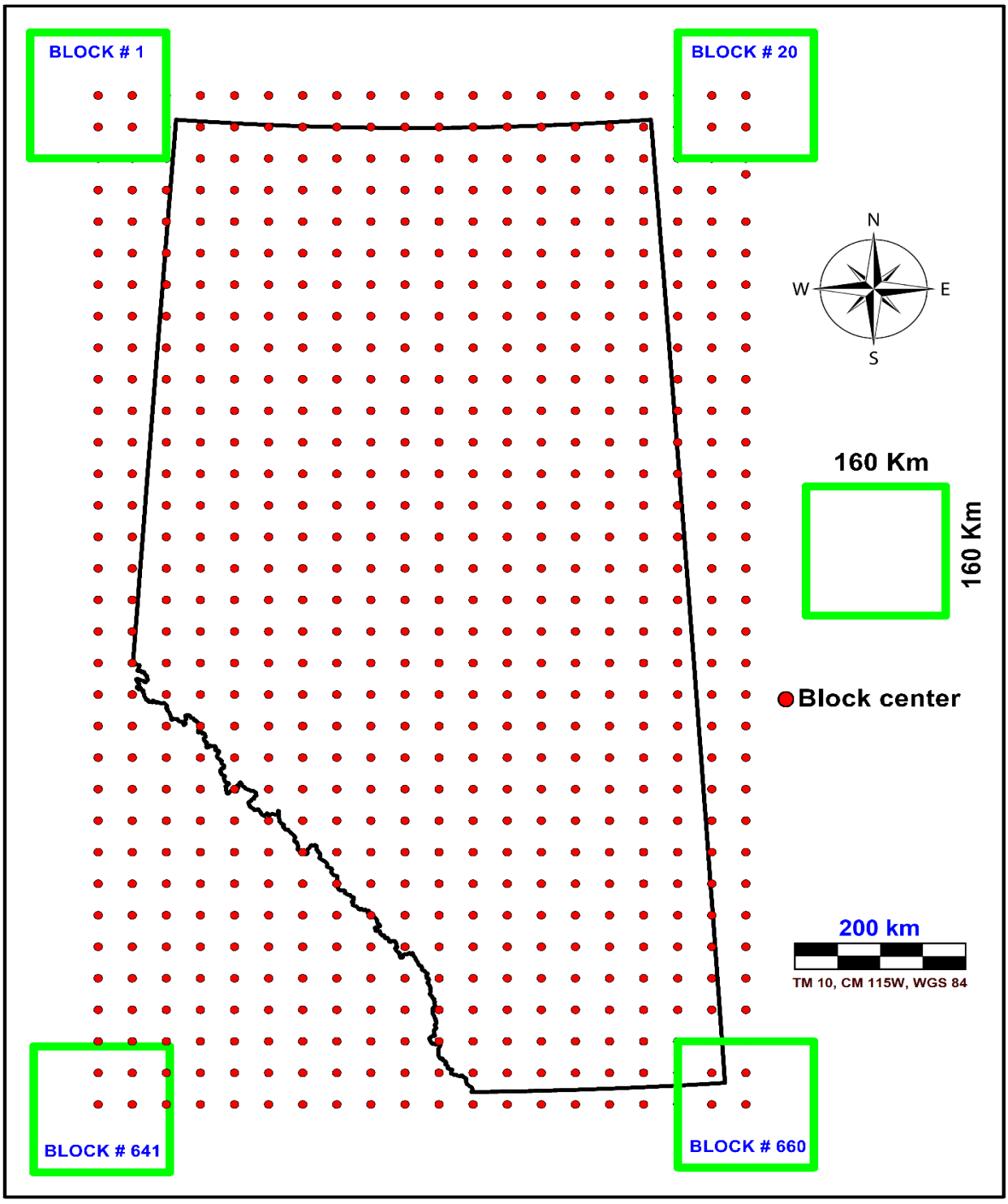

Figure 7. Layout of the centers of the 660 blocks selected for CPD computation.

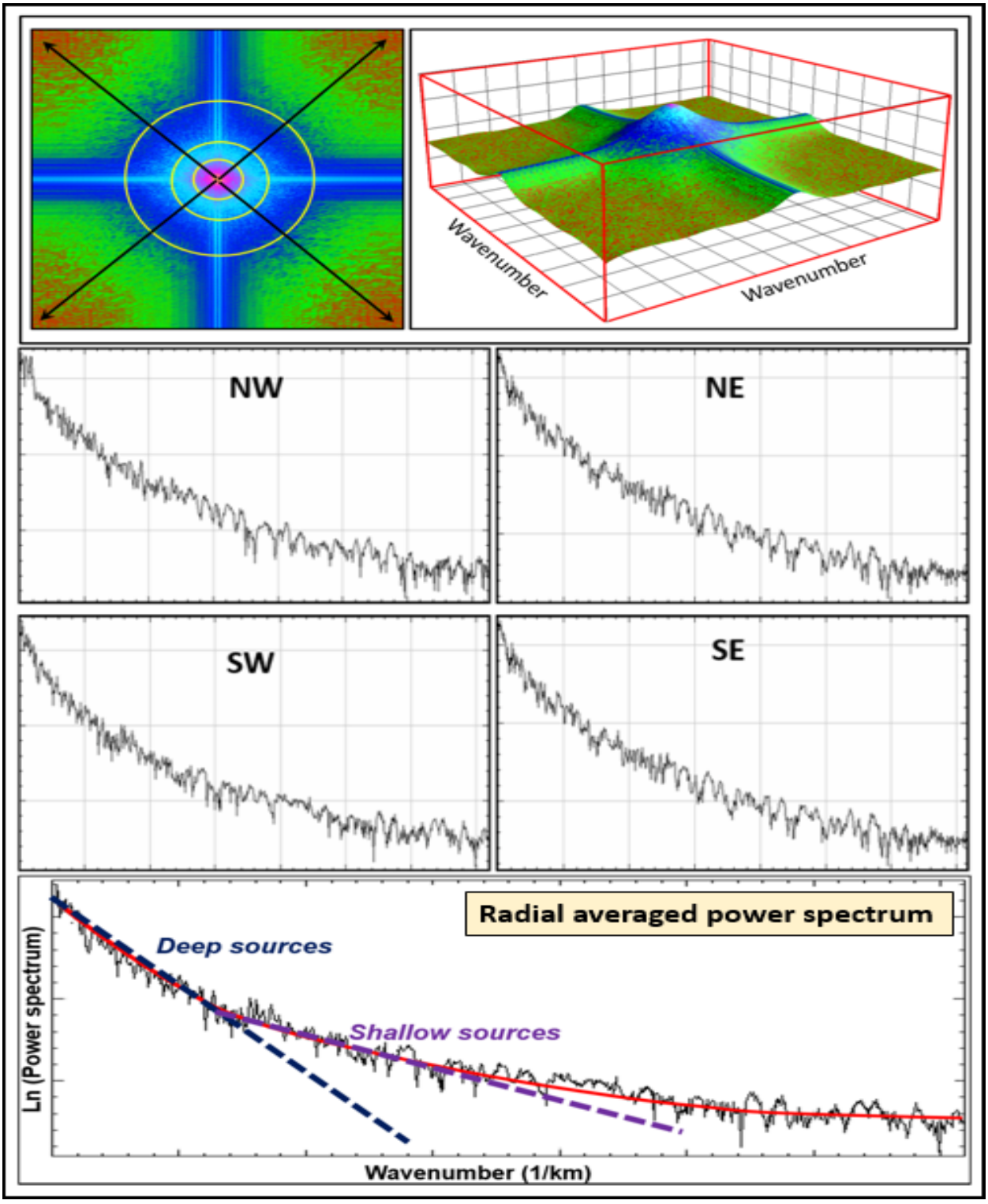

Figure 8. Example of FFT-based radial averaged power spectrum.

Using the FFT-based spectral analysis method, the depth of the magnetic source is derived from the slope of the natural log of the power spectrum plotted against the wavenumber (Figure 8). Since DBMS lies deep within the Earth's crust, it generates long-wavelength magnetic anomalies with steep slopes on the power spectrum curve. A steeper slope corresponds to a deeper magnetic source. The magnetization model employed assumes magnetic anomalies arise from a single horizontal layer (Figure 9) with thickness Δz, confined between the depths of the top (Z_t) and bottom (Z_b). The depths to the top and bottom of the magnetic source can thus be determined using curve-fitting techniques applied to the spectral shape of magnetic anomalies.

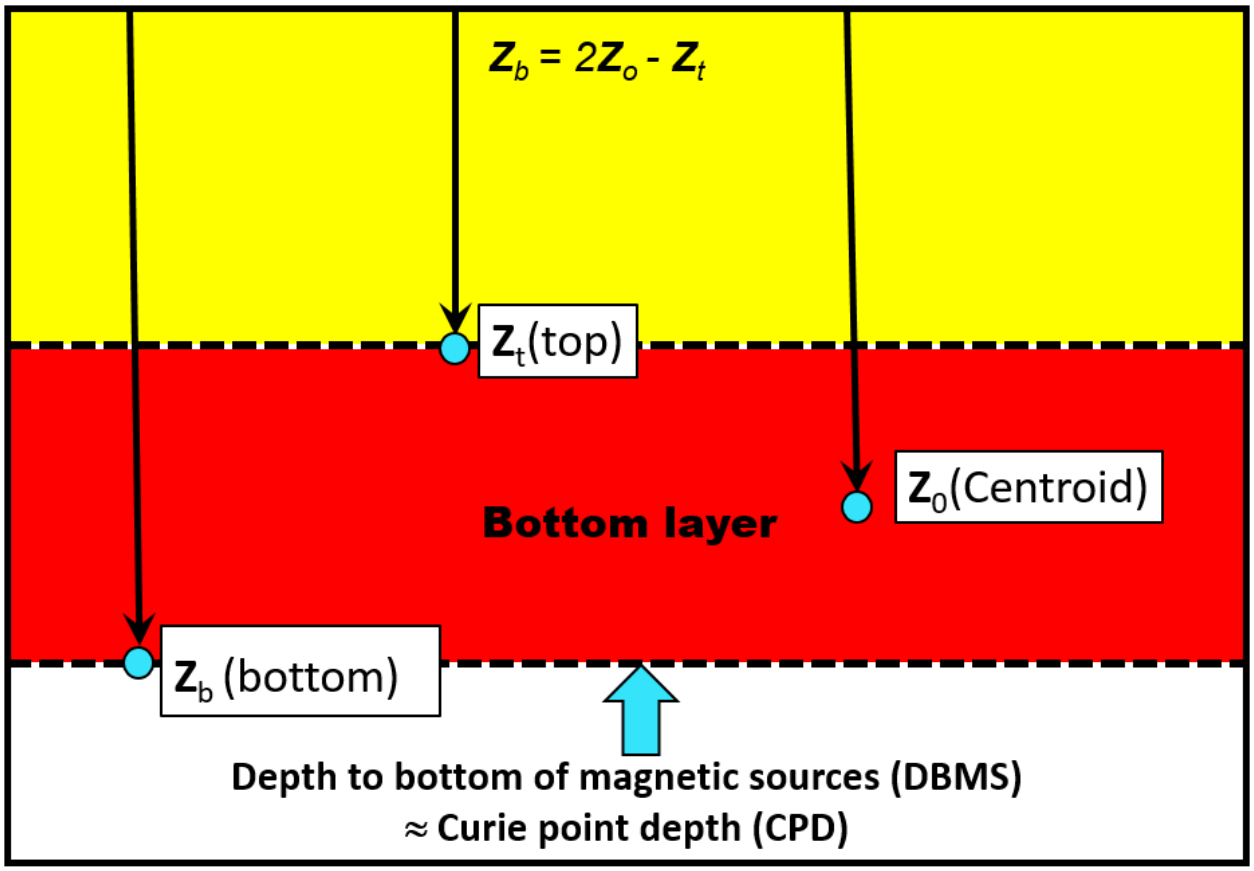

Figure 9. A diagram showing the locations of Zt, Zo and Zb relative to bottom magnetic layer.

The method introduced by Spector and Grant (1970) initially estimated the depth to the top (Z_t) of magnetized layers using the slope of the radially averaged power spectrum.

This approach was later modified by Bhattacharyya and Leu (1975, 1977) to calculate the depth to the centroid (Z_o) of the magnetic layer (Figure 9). By combining these two depths (Z_t and Z_o), Okubo *et al*. (1985) proposed a procedure to estimate the depth to the bottom of magnetic layers (Z_b), which represents the depth to the Curie isotherm surface.

Typically, DBMS computation assumes an uncorrelated and random distribution of magnetization within magnetic sources (Bhattacharyya and Leu, 1975; Okubo *et al*., 1985; Tanaka *et al*., 1999). Consequently, the results are stochastic and may exhibit some ambiguity. However, recent studies (Maus *et al*., 1997; Bansal *et al*., 2011; Li *et al*., 2017) suggest that magnetization within magnetic sources demonstrates fractal behavior, characterized by repeating patterns at varying scales.

This study employed two approaches to estimate the CPD isotherm:

1. **Centroid Approach:** Assumes the magnetization of sources is uncorrelated and random (Okubo *et al*., 1985; Tanaka *et al*., 1999).

2. **Fractal Approach:** Incorporates self-similarity or fractal behavior in the power spectrum ($P(k) = k^{\beta}$), thus requiring correction (Pilkington and Todoeschuck, 1993; Maus and Dimri, 1994; Maus *et al*., 1997; Fedi *et al*., 1997). Mandelbrot (1983) described the concept of self-similarity, indicating that data appears consistent across scales.

In both approaches, the depth to the Curie isotherm surface (Z_b) is derived from two slopes on the power spectrum curve: one representing the depth to the centroid (Z_o) and another for the depth to the top (Z_t) of the magnetic source (Figure 10). These depths are combined using the formula: $Z_b = 2Z_o - Z_t$ as shown in Figure 9.

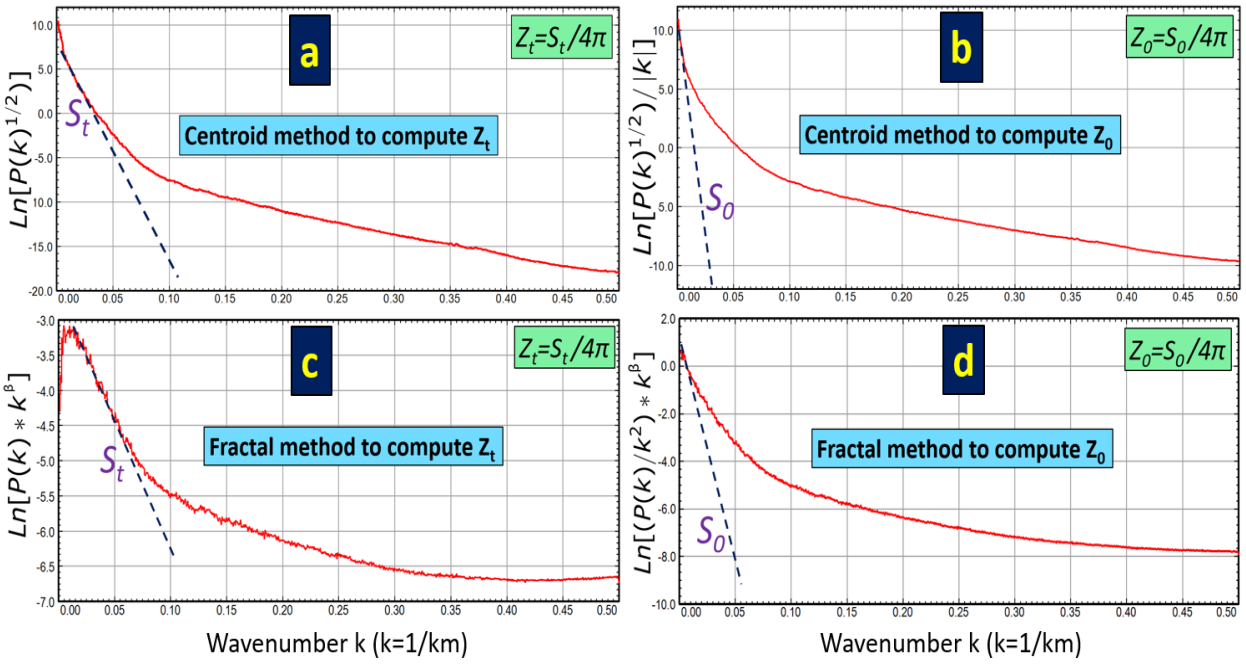

Figure 10. Power spectrums of magnetic data showing the centroid and the fractal approaches to compute Z_t and Z_o.

The magnetization models utilized in these methods assume magnetic anomalies arise from a single horizontal layer extending infinitely in all directions, with thickness Δz confined between two depths: top (Z_t) and bottom (Z_b). For such layers, the depths can be estimated using the equations provided by Blakely (1996) through spectral analysis of magnetic anomalies (Equation 1).

$$P(k_x, k_y) = 4\pi^2 C_m^2 |\phi_m|^2 |\phi_f|^2 * e^{-2|k|Z_t}(1 - e^{-|k|(Z_b - Zt)}) \qquad (1)$$

Where:

$P(k_x, k_y)$ is the power spectrum of magnetic data,

k_x and k_y are the respective wavenumbers in x- and y-directions,

C_m is the magnetic proportionality constant,

φ_M is the power-density spectra of the total-field magnetic anomaly,

Φm power spectrum of magnetization

Φf power spectrum of geomagnetic field

Z_t and Z_b are the top and bottom depths of magnetic layer, respectively,

Φ_m and Φ_f become constant when taking the radial average. Assuming random magnetization, the radial averaged power spectrums expressed in Equation (1) can be simplified into the following formula (Zhou and Thybo, 1998; Tanaka *et al*., 1999):

$$P(k) = A * e^{-2|k|Z_t}(1 - e^{-|k|(Z_b - Z_t)})^2 \qquad (2)$$

Where:

P(k) is the power spectrum,

A is a constant value,

k is the wavenumber (k=1/wavelength),

Z_t is the depth to top of magnetic source, and

Z_b is depth to bottom of magnetic source.

Equation 2 is used as a basis to derive Equations 3 and 4 below.

Centroid Method

The DBMS (Z_b) using the centroid approach (Okubo *et al*., 1985; Tanaka *et al*., 1999) was calculated as described in the following steps:

1. Estimate the depth to the top of the deepest magnetic source (Z_t) that can be detected on the power spectrum (Figure 10a) using Equation 3 below:

$$Ln[P(k)^{1/2})] = A_t - |k|Z_t \qquad (3)$$

2. Estimate the depth to the centroid of the magnetic source (Z_o) from the power spectrum (Figure 10b) using Equation 4 below.

$$Ln[P(k)^{1/2})/K] = A_0 - |k|Z_0 \qquad (4)$$

3. Calculate the depth to the bottom of the magnetic source (Z_b) using the following equation:

$$Z_b = 2Z_0 - Z_t \qquad (5)$$

The computed Z_b values in Equation (5) represent the estimated CPD isotherm surface underneath the study area (Figure 11).

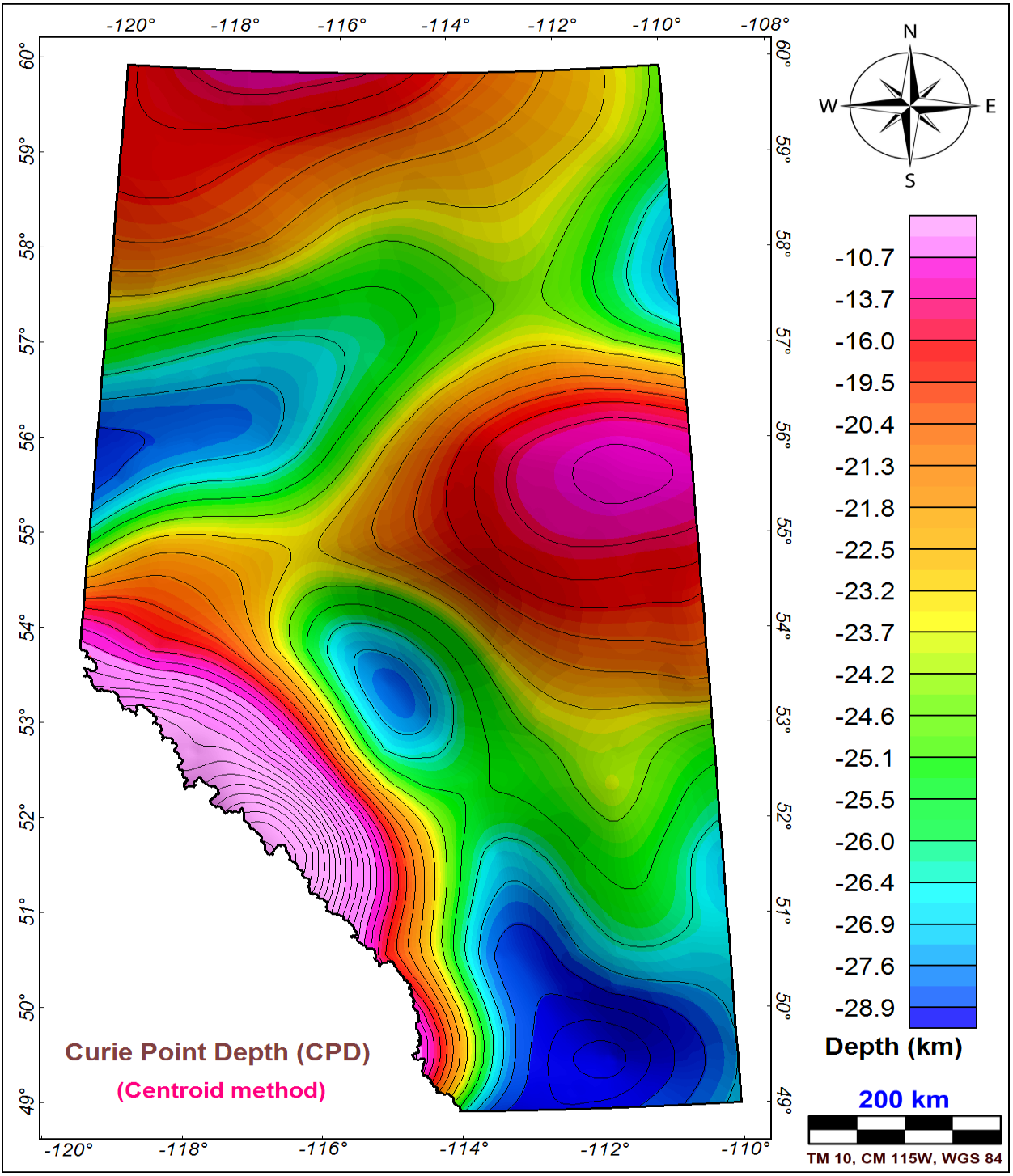

Figure 1. Curie point depth (CPD) computed using centroid method.

Fractal Method

Traditional methods for calculating CPD from power spectrum analysis often assume uniform or simple distributions of magnetization. While this simplification may work for areas with straightforward geological features, it tends to oversimplify the Earth's crust's complexity. As a result, these methods are better suited to regions with simple geology.

In contrast, fractal methods provide more accurate results in areas with complex geological structures. These methods consider the fractal distribution of magnetic sources, which is often a more realistic representation in geological contexts. They offer more precise CPD estimates compared to traditional methods. However, fractal methods are computationally more demanding than the centroid method (Pilkington *et al*., 1994).

To apply the fractal method, we followed the same steps outlined in the centroid method. However, instead of Equations 3 and 4, we utilized Equations 6 and 7 to calculate Z_t (Figure 10c) and Z_o (Figure 10d), respectively.

$$Ln[P(k) * k^{\beta}] = A - 2\,|k| Z_t \qquad (6)$$

$$Ln[(P(k)/k^2) * k^{\beta}] = A - 2\,|k| Z_0 \qquad (7)$$

The CPD isotherm surface derived from the fractal approach, is displayed in Figure 12.

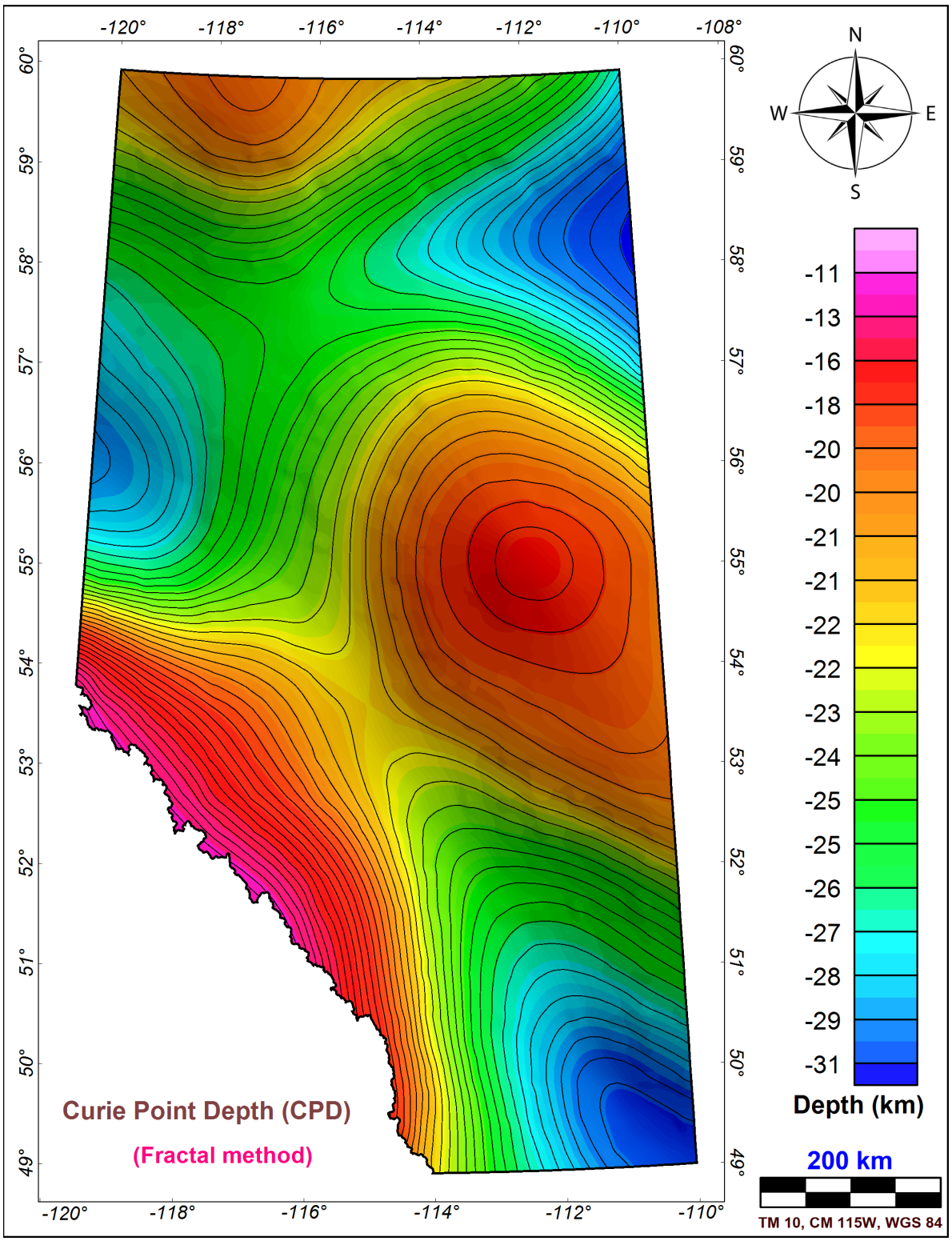

Figure 2. Curie point depth (CPD) computed using fractal method.

A key challenge of the fractal approach lies in the selection of the fractal exponent (β). Determining β is not straightforward, as it cannot be estimated independently, and its value varies depending on the geological complexity of the area.

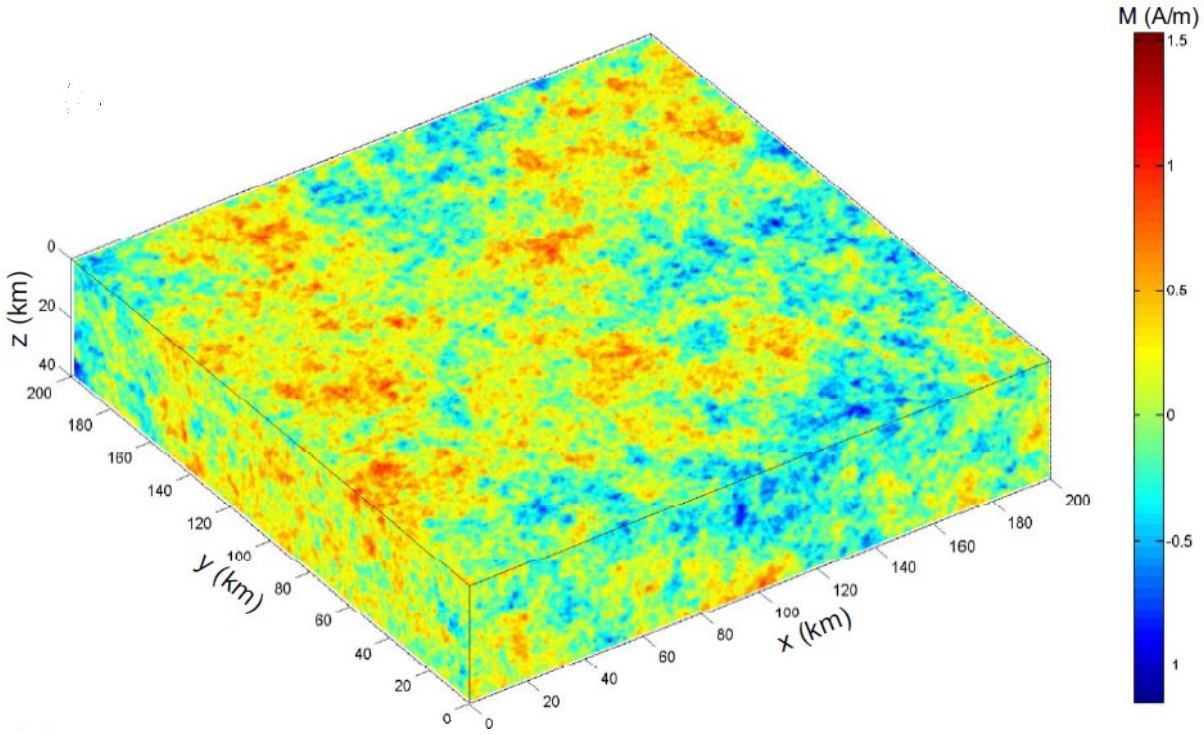

Figure 3. Synthetic 3-D fractal magnetization model (Li et al, 2013).

To address this limitation, several researchers (e.g., Pilkington and Todoeschuck, 1993; Maus *et al*., 1997; Bouligand *et al*., 2009; Li *et al*., 2013) developed synthetic 3-D fractal magnetization models, such as the one depicted in Figure 13. These models simulate the Earth's crustal magnetization by incorporating fractals to replicate the complex, self-similar patterns characteristic of natural geological formations. As a result, these synthetic models provide a more realistic representation of crustal magnetization. Additionally, they enable the estimation of fractal model parameters by fitting a theoretical power spectrum curve to the calculated radial power spectrum derived from RMI magnetic data. In this study, we utilized the 3-D synthetic model (Figure 13) proposed by Li *et al.* (2013) to compute the fractal CPD depth parameters.

The procedure of fitting the theoretical (synthetic) power spectrum generated from 3D fractal synthetic model with the RMI power spectrum using Block # 316 as an example, is illustrated in Figures 14, 15 and 16, respectively. The best fit was observed when the fractal exponent β is equal to 4.3 (Figure 16).

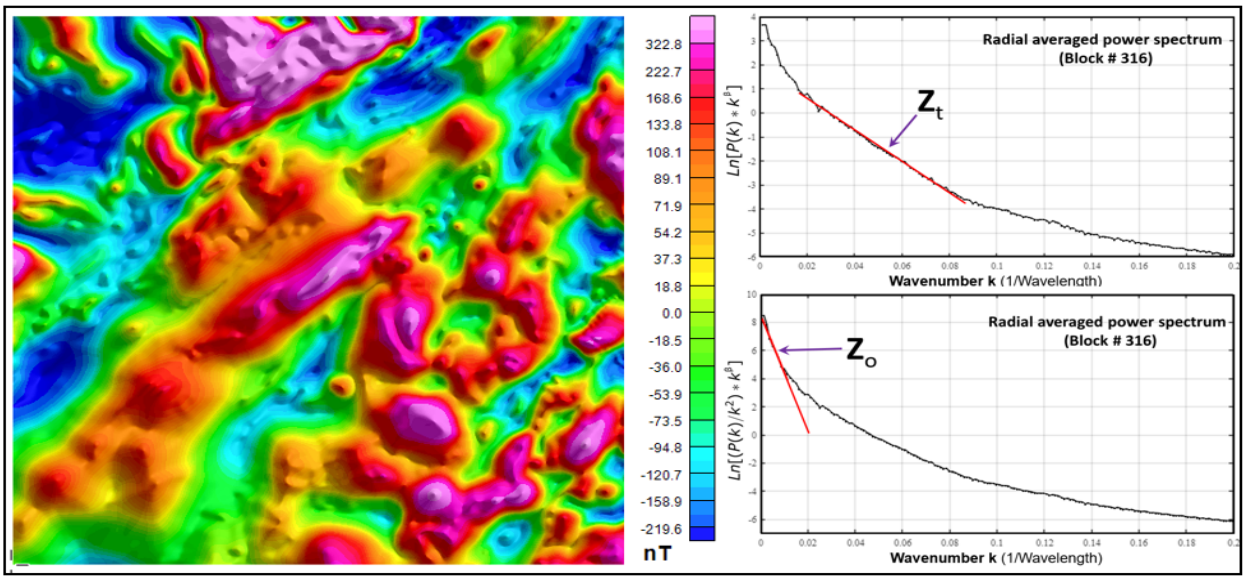

Figure 4. Radial average power spectrum generated for Block # 316.

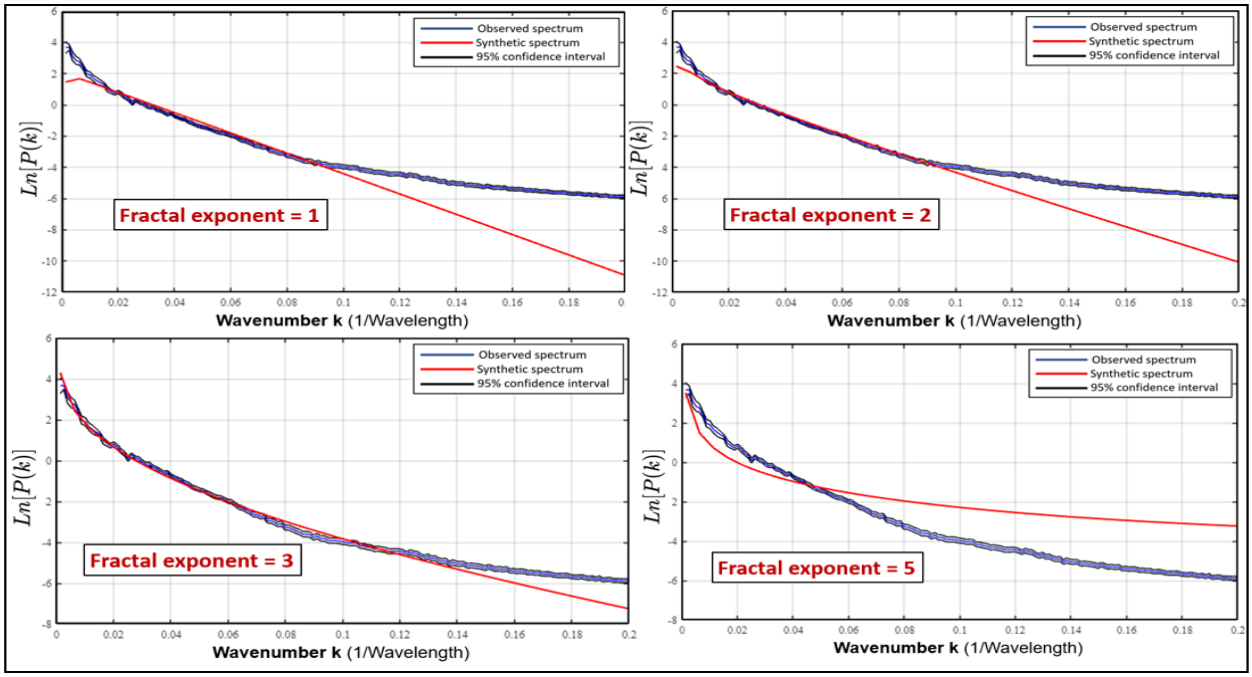

Figure 5. Fitting power spectrum of Block # 316 to synthetic power spectrum with various fractal exponents extracted from synthetic 3-D fractal magnetization model of Li et al., 2013.

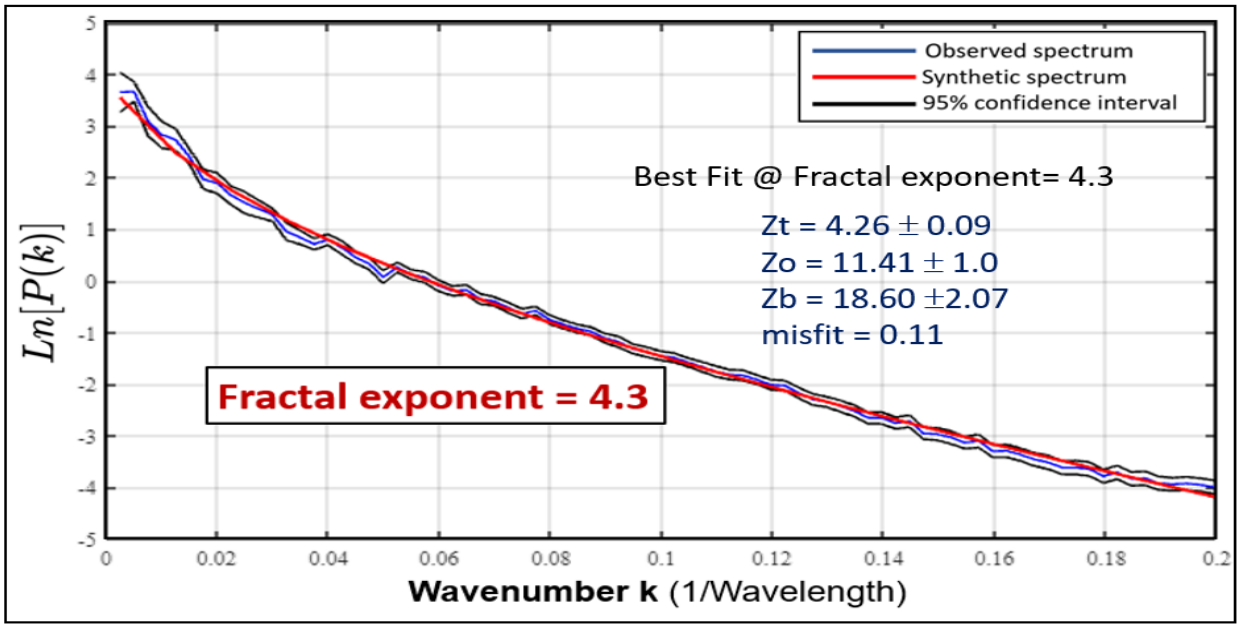

Figure 16. Best fit of Block # 316 power spectrum with synthetic power spectrum when fractal exponent β = 4.3. At this fit, the depth to CPD is equal to 18.6 β 2.07 km.

CPD Derived Average Geothermal Gradient

Geothermal gradient is the rate of change in temperature with respect to increasing depth in Earth's interior. Significant shallow variability in geothermal heat exists due to hydrodynamic flow, crustal heat sources and mantle heat sources. The average geothermal gradient for the center of the block is displayed in Figure 17. It is important to recognize that this method simply takes the average gradient to CPD depth and makes no consideration for shallow variability. Therefore, we are not showing true geothermal gradient maps, rather CPD derived average geothermal gradient maps. The CPD derived average geothermal gradient is proportional to deep mantle derived heat sources and thus can be used as a background heat trend.

After computing the CPD isotherm using the centroid and fractal methods, we applied Equation 8 from Turcotte and Schubert (1982) to estimate the CPD-derived average geothermal gradient, assuming a surface temperature (T_S) of zero and a Curie temperature (T_c) of pure magnetite averaging 580°C.

$$Geothermal\ gradient(^{\circ}C/km) = \frac{T_C - T_S}{Z_b} = \frac{580}{Z_b} \qquad (8)$$

CPD derived average geothermal gradient maps are shown for the centroid CPD (Figure 18) and the fractal CPD (Figure 19) respectively.

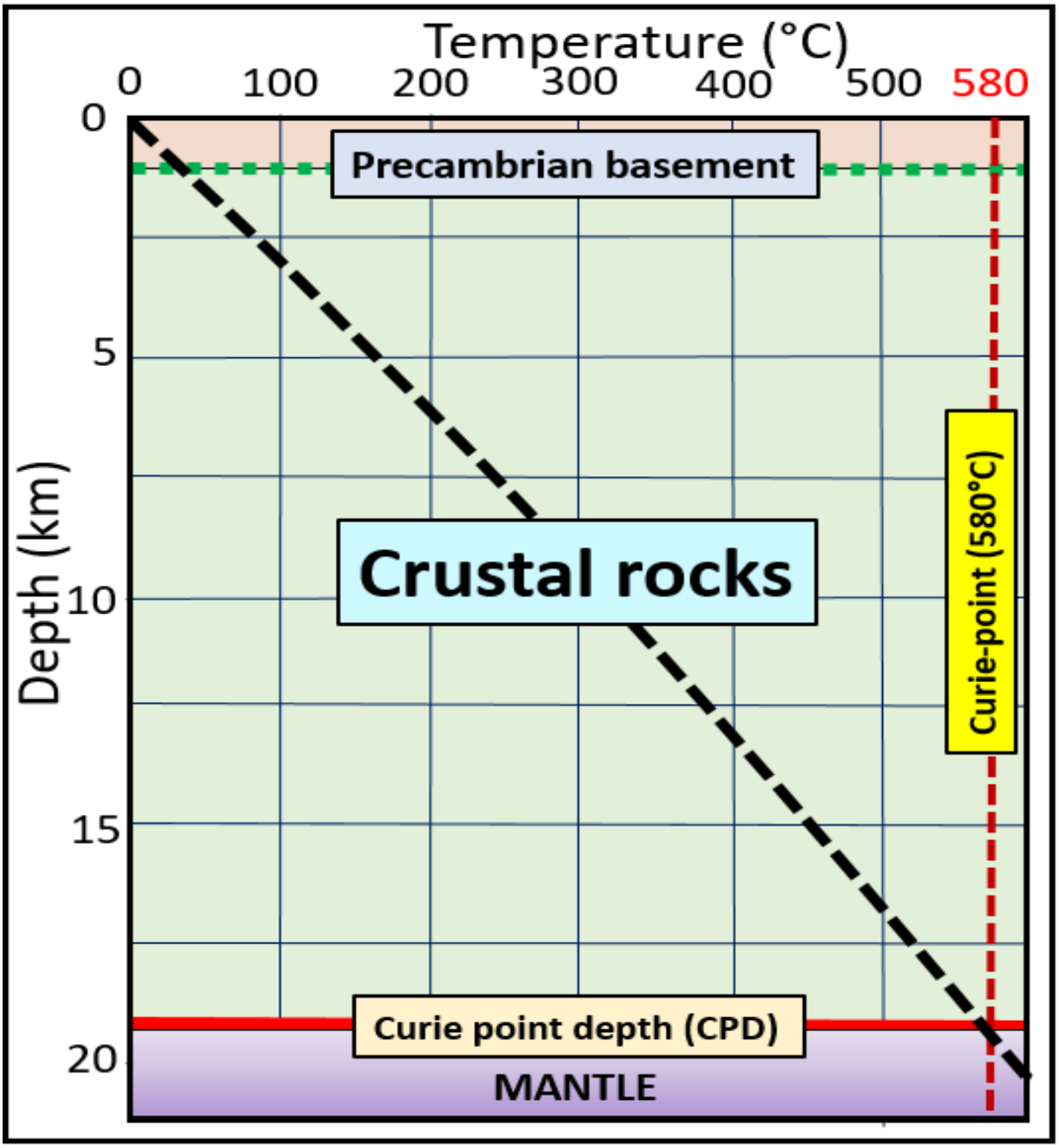

Figure 17. Geothermal gradient at the center of Block # 316.

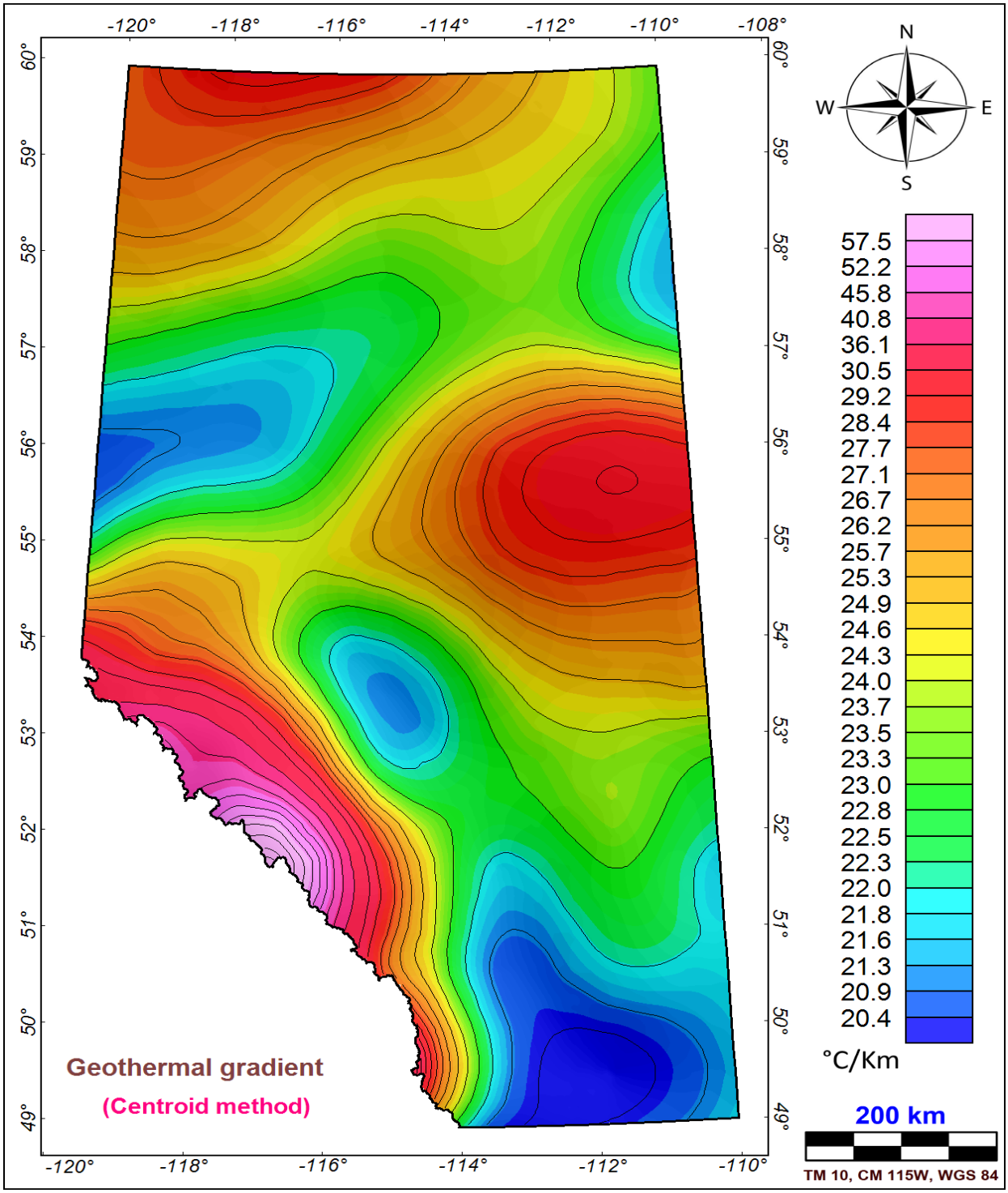

Figure 38. CPD derived average geothermal gradient computed using the centroid method.

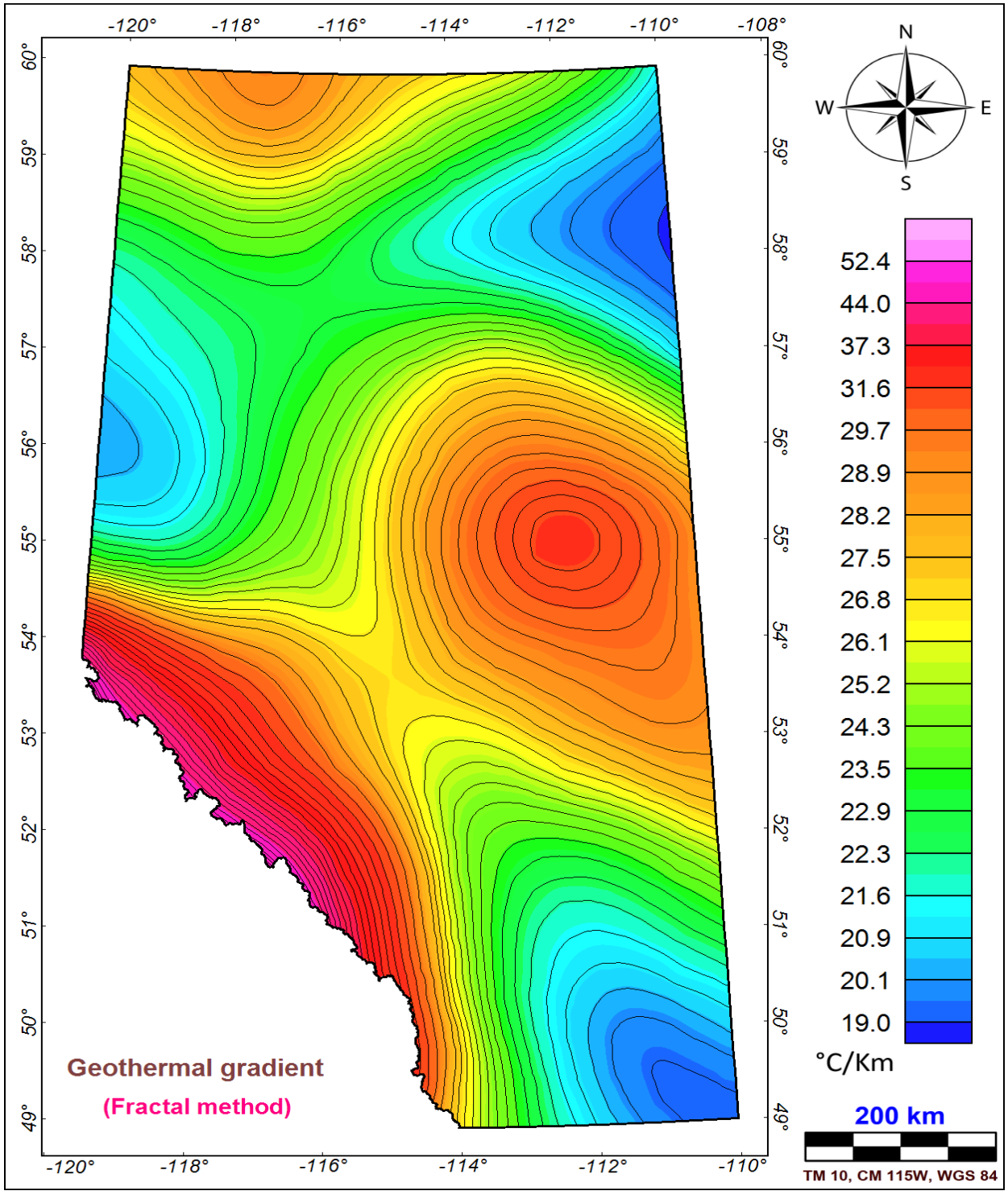

Figure 9. CPD derived average geothermal gradient computed using the fractal method.

CPD Derived Average Heat Flow

Heat flow is the movement of heat from the earth's interior to the surface of the earth. Without any localized information on shallow heat sources or variability in conductivity, heat flow becomes proportional to the geothermal gradient.

We computed heat flow maps for the study area using Equation (9) below:

$$Heat\ flow\ (Q) = \lambda * \frac{580^{\circ}C}{Z_b} \qquad (9)$$

Where:

λ is the thermal conductivity.

In this study, we used λ = 2.5 W/m·C, the average value for crustal rocks. Using Equation (9), we computed a CPD derived average heat flow map from both the fractal and centroid maps (Figures 20 and 21, respectively).

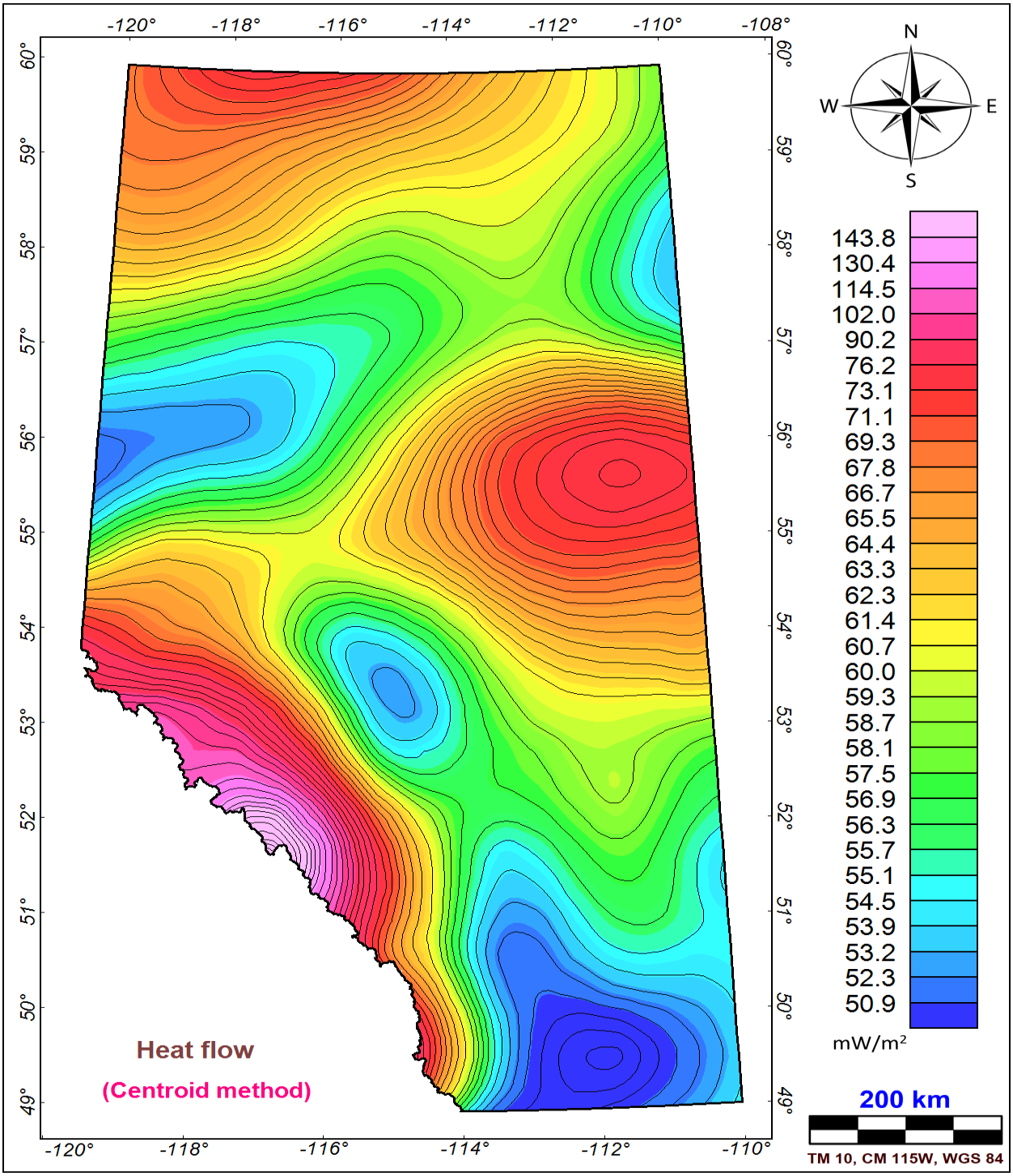

Figure 4. CPD derived average heat flow of the study area computed using centroid method.

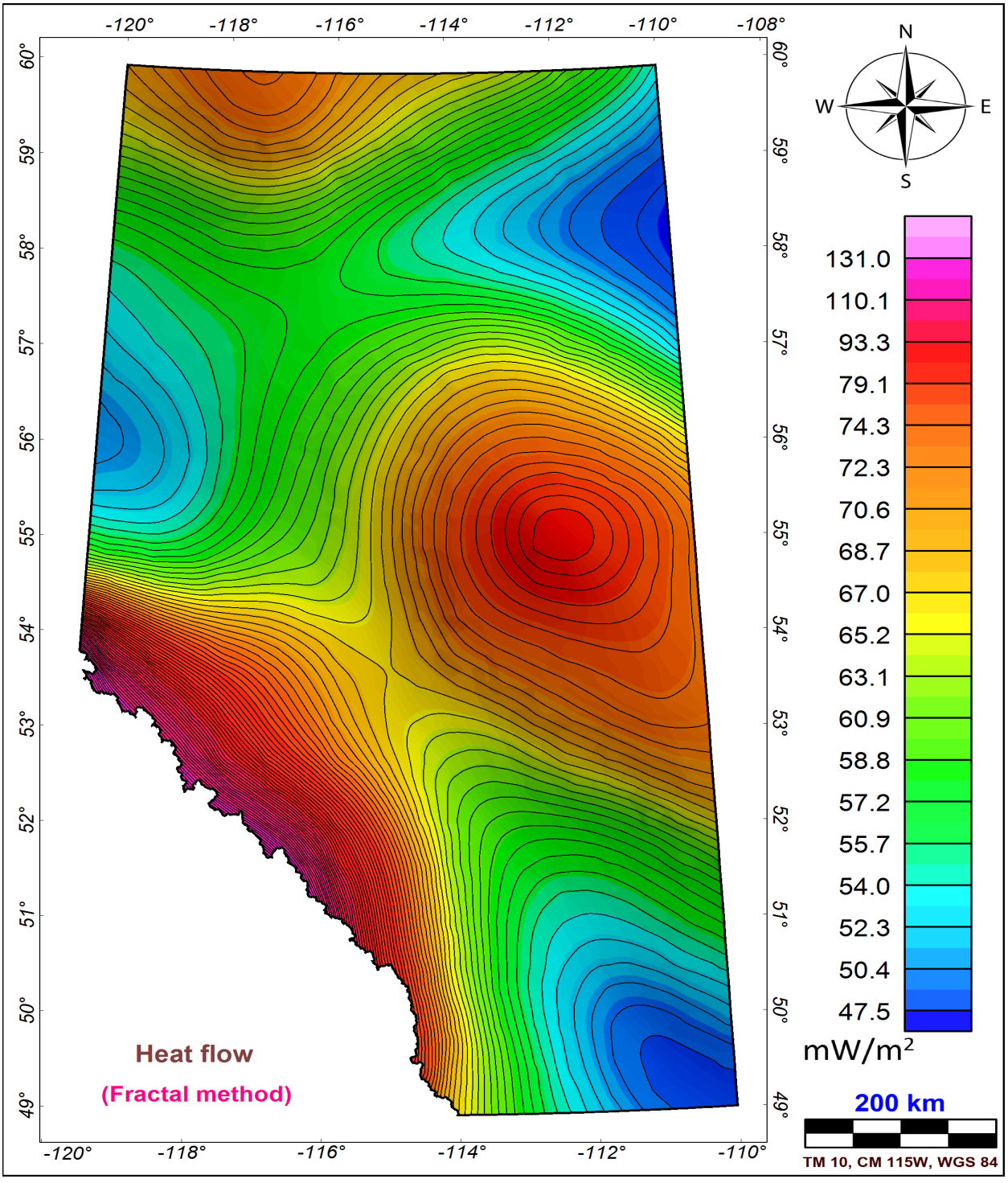

Figure 21. CPD derived average heat flow of the study area computed using fractal method.

3D gravity inversion to map Moho surface

To explore the potential relationship between the CPD isotherm and the depth of the Moho within the study area, a 3D gravity structural inversion was applied to the gravity data (Figure 6). The inversion in this analysis does not account for lateral variations in the density distribution of crustal rocks, as it assumes a constant density.

For this study, FFT-based methods derived from the algorithms of Parker (1973) and Oldenburg (1974) were implemented using a Matlab code developed by Gomez-Ortiz *et al.* (2005). In 1973, Parker introduced an FFT-based algorithm for forward modeling of gravity data. By using Parker's formula (Equation 10), the gravity anomaly caused by an uneven, uniform material layer can be calculated through a series of Fourier transforms.

$$F[(\Delta g(x,y)] = -2\pi G\,\Delta\rho * e^{(-kh_0)} \sum_{n=1}^{\infty} \frac{k^{n-1}}{n!} F[h^n(x,y)] \qquad (10)$$

Oldenburg (1974) later rearranged Parker's forward modeling algorithm into Equation (11), enabling the depth to the density interface, or Moho, to be computed from gravity anomaly grids through an iterative process. The gravity inversion algorithm developed by Oldenburg, utilized in this study, is outlined below.

$$h(x,y) = F^{-1}\left[\frac{F[\Delta g(x,y)]e^{(-kh_0)}}{-2\pi G\,\Delta\rho} - \sum_{n=2}^{\infty} \frac{|k|^{n-1}}{n!} F[h^n(x,y)]\right] \qquad (11)$$

Where:

F(Δg) is the Fourier transform of the gravity anomaly,

G is the gravitational constant,

Δr is the density contrast across the Moho surface,

k is the wavenumber (k=1/wavelength),

h(x,y) is the depth to the Moho (positive downward),

h_0 is the mean depth of the horizontal interface (i.e., Moho)

Equation (11) enables for the determination of Moho topography through an iterative inversion procedure. This method assumes a mean depth of the Moho (h_0) and the density contrast ($\Delta\rho$) between the Moho and the overlying crustal rocks. Based on the CRUST1.0 global crustal model, the depth to the Moho interface within the study area is approximately 43 km below sea level. A density contrast of 0.42 g/cm^3 was applied, based on an average density of 2.93 g/cm^3 for the lower crust and 3.35 g/cm^3 for the upper mantle (Kaban and Mooney, 2001). The model was refined using 100 iterations (Figure 22), beyond which the difference between the calculated Bouguer gravity and the observed gravity remained nearly unchanged. The resulting depth to Moho map is shown in Figure 23. The error resulting from this fit is presented in Figure 24.

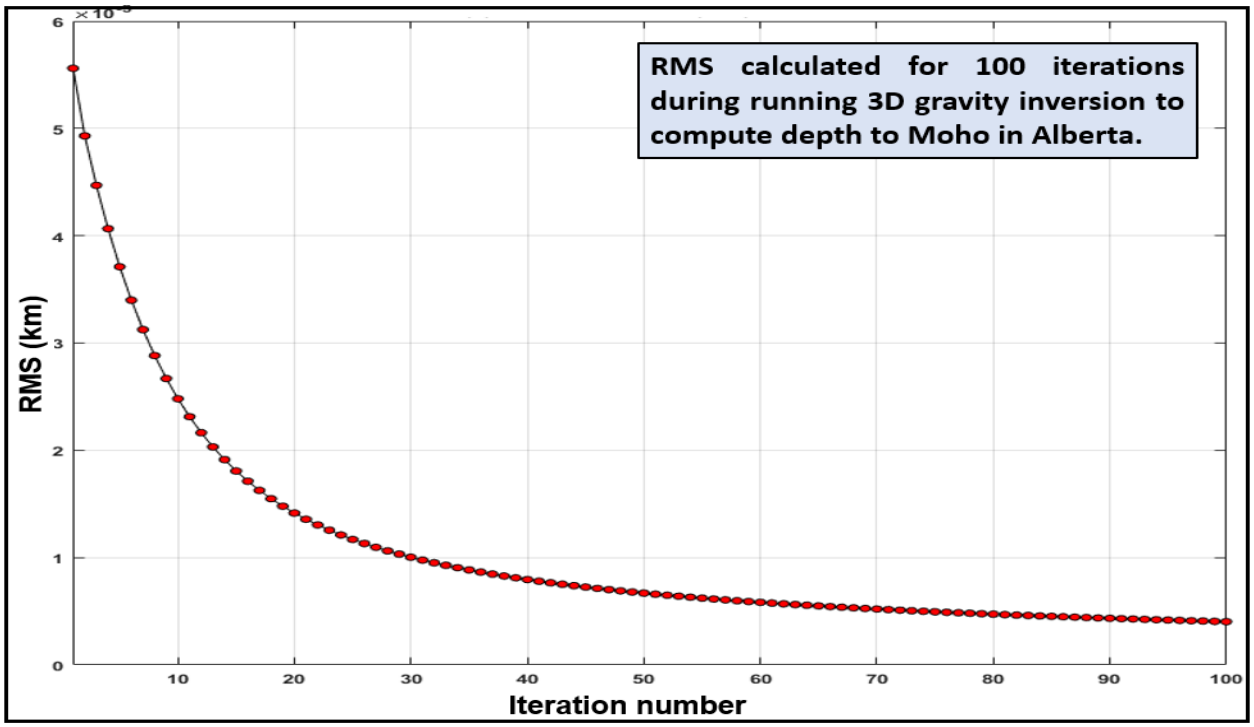

Figure 22. Root mean square (RMS) generated through 3D gravity inversion.

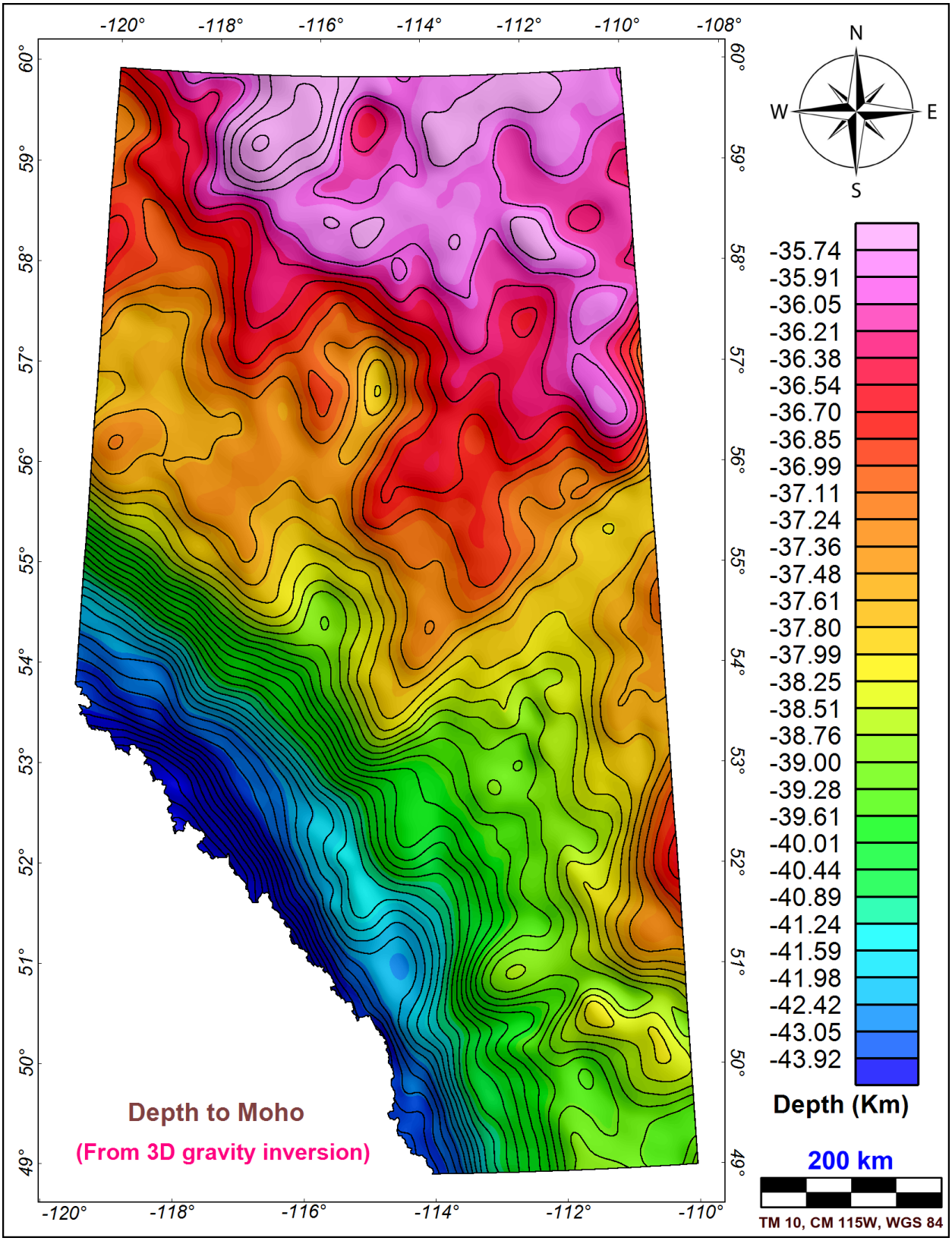

Figure 3. Depth to Moho of Alberta computed from 3D inversion of Bouguer gravity.

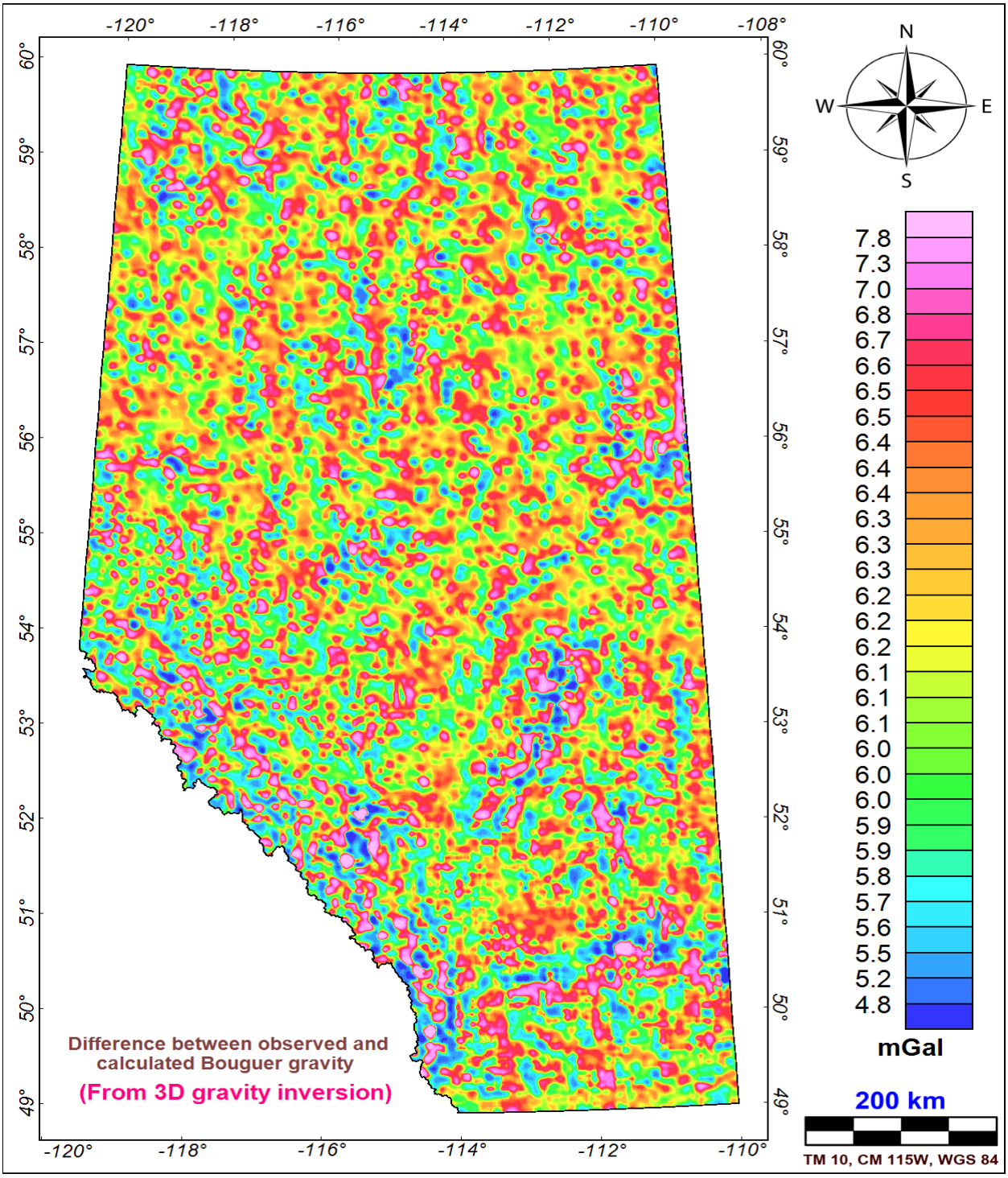

Figure 54. 3D gravity inversion misfit errors (Observed Bouguer minus calculated Bouguer).

Results indicate that the Moho depth ranges from 35 km to 45.6 km, with an average depth of 38.3 ± 2.2 km below sea level. It is relatively shallow in northeastern Alberta (~35 km) and gradually deepens (~45.6 km) towards southwestern Alberta.

Statistical analysis comparing the inverted Moho surface with the computed CPD isotherm surface reveals a moderate negative correlation (correlation coefficient ~ -0.70). This negative relationship may occur due to the heat-retention properties of crustal rocks with low thermal conductivity, which contribute to a shallow CPD despite the presence of a deep Moho. Such thermal patterns are typically observed in ancient cratons, including the Canadian Shield. In these regions, the crust is thick, resulting in a deep Moho. However, low-conductivity rocks retain heat efficiently, leading to the development of a shallow CPD.

While positive correlations between Moho and CPD depths have been documented in certain regions, recent studies, such as Li *et al.* (2019), propose that CPD depths are independent of Moho depths. This independence stems from the distinct characteristics of the two boundaries: the Moho represents a lithological boundary, whereas the CPD signifies a thermal boundary.

RESULTS

The methodology used in this study to compute the CPD involved 660 overlapping magnetic blocks. Among these, 417 are located within Alberta, with the findings summarized in Table 1. On average, the CPD isotherm surface derived from both the centroid and fractal methods is approximately the same, at a depth of 23.4 ± 3.5 km. However, the CPD determined through the centroid approach appears to be slightly deeper than that obtained through the fractal method. Specifically, the mean CPD depth calculated using the centroid method is 23.7 ± 3.3 km, while the depth derived from the fractal method is 23.0 ± 3.6 km.

Overall, CPD is relatively shallow in southwestern Alberta (approximately 15 km), particularly beneath the Rocky Mountain Belt. In contrast, the CPD is generally deeper under the Interior Plains region, with depths of about 25.0 km under the Rae Craton and 27.0 km beneath the southeastern portion of the Hearne Craton. Notably, along the Snowbird Tectonic Zone (SBTZ), located between the Alberta Basin and the Hearne Craton, the CPD appears shallower, at around 20 km.

The CPD, CPD derived average geothermal gradient, and CPD derived average heat flow computed in this study do not account for radiogenic heat generated by uranium (U), thorium (Th), and potassium (K) within granitic rocks of the Precambrian basement. Radiogenic heat is reported to be significantly high in the Precambrian crystalline basement rocks beneath the Western Canada Sedimentary Basin, particularly under the Rocky Mountains (e.g., Majorowicz and Weides, 2013; Hyndman, 2023).

Comparing the CPD results to a global reference dataset developed by Li et al 2017, some differences are observed specifically in the area of the Rocky Mountains. The Li et al. 2017 model is based on regional, satellite derived magnetic data. Thus, we have higher confidence in our new model due to higher quality input data.

CPD derived average geothermal gradient (average 25.6 ± 5.0 ^{o}C/km) and heat flow trends align loosely with existing regional heat flow and geothermal gradient data for Alberta (Bachu and Burwash, 1994). This is interesting because the Bachu dataset is weighted towards well information and shallow heat observations not necessarily linked directly to the mantle derived heat. Furthermore, the Lucazeau (2019) global heat flow dataset shows similar heat flow values to our results.

Additionally, the depth to the Moho, as determined through 3D gravity inversion, ranges from 35.0 km to 45.6 km, with an average depth of 38.3 ± 2.2 km. The mantle exhibits shallower depths in northeastern Alberta, while it deepens in the southwestern region. Interestingly, these trends contrast with the observed CPD depths across Alberta.

Table 1. Statistical summary of results obtained in this study.

Measured data	Minimum	Maximum	Mean	Std deviation
CPD Centroid (km)	8.1	30.5	23.7	3.3
CPD Fractal (km)	12.1	30.3	23.0	3.6
AVERAGE CPD (km)	**10.1**	**30.4**	**23.4**	**3.5**
Geothermal gradient centroid (°C/km)	19.0	71.3	25.20	5.4
Geothermal gradient fractal (°C/km)	19.1	47.8	25.90	4.6
AVERAGE GEOTH. GRADIENT (°C/km)	**19.1**	**59.6**	**25.6**	**5.0**
Heat flow centroid (mW/m^2)	47.6	178.2	63.0	13.4
Heat flow fractal (mW/m^2)	47.8	119.5	64.8	11.6
AVERAGE HEAT FLOW (mW/m^2)	**47.7**	**148.9**	**63.9**	**15.5**
Depth to Moho (km)	35.0	45.6	38.3	2.2

CONCLUSIONS

This study demonstrates how magnetic data can provide valuable indirect insights into the regional distribution of geothermal energy by determining the depth to the bottom of magnetic sources (DBMS) from the radial power spectrum of magnetic data. The DBMS surface corresponds to the CPD isotherm surface, which both coincide at the Curie point temperature of 580°C. At this depth, crustal rocks lose their magnetization, marking the boundary of magnetic sources.

Using this principle, the CPD isotherm surface was indirectly mapped through the FFT-based radial averaged power spectrum of residual magnetic intensity (RMI) data. Two established methods were applied: the centroid method and the fractal method. The centroid method assumes random, uncorrelated magnetization sources, while the fractal approach assumes the self-similarity of the power spectrum and includes necessary corrections.

The estimated CPD isotherms range from 8.1 to 30.5 km in depth (centroid method) and 12.1 to 30.3 km (fractal method), both with an average depth of approximately 23.7 ± 3.3 km and 23.0 ± 3.6 km, respectively. Although the results are broadly similar, the centroid approach generally yields slightly deeper CPD estimates than the fractal method.

Regionally, CPD depth computed in Alberta varies significantly. In southwestern Alberta, particularly under the Rocky Mountain Belt, depths are relatively shallow (~15 km). By contrast, deeper CPD depths are found in the cratons of the Interior Plains (~25 km beneath the Rae Craton and ~27 km under the Hearne Craton). The Snowbird Tectonic Zone (SBTZ) exhibits elevated CPD isotherms, with shallower depths of ~20 km at the edge between the Alberta Basin and Hearne Craton.

Furthermore, the CPD derived average geothermal gradient and heat flow values for Alberta, as shown in Table 1 align well with existing regional geothermal gradient and heat flow data determined in previous studies (e.g., Majorowicz and Grasby, 2010b). However, the calculated CPD, geothermal gradient, and heat flow do not account for radiogenic heat generated by uranium, thorium, and potassium within granitic rocks abundant in the Precambrian crystalline formations beneath the Western Canada Sedimentary Basin (e.g., Majorowicz and Weides, 2014, Hassan & Harms, 2024b) or higher frequency near surface variability expected due to localized geological variability.

Interestingly, the CPD depth estimated in the Canadian Rocky Mountains (~ 15 km) agrees with previous studies (e.g., Gaudreau *et al*., 2019) and is supported by the finding from several studies on high thermal anomalies beneath the Rocky Mountains (Hyndman and Lewis, 1999; Hyndman and Currie, 2011; Hyndman, 1923).

Several geological and thermal characteristics contribute to the shallow CPD isotherm observed in the Rocky Mountain Belt:

1. **Thin lithosphere**: The lithosphere beneath the Canadian Rockies is relatively thin, allowing heat from the mantle to reach the surface more easily (Hyndman, 2010).

2. **Small-scale mantle convection**: Convection currents in the mantle beneath the Rockies contribute to elevated temperatures, with mantle temperatures reaching 800–900°C at the Moho (Hyndman, 2010; Bao *et al*., 2014).

3. **Tectonic activity**: The region's tectonic activity, including the interaction of the North American Plate with other tectonic plates, generates heat through friction and deformation (Hyndman, 2010).

4. **Heat production from radioactive decay**: Radiogenic heat generated from the decay of radioactive elements such as uranium (U), thorium (Th), and potassium (K) in the crust increases the temperature within the crust, leading to higher heat flow. This elevated temperature can cause the Curie isotherm to be shallower. The heat production under the Cordillera ranges between 2.0 and 5.0 mW/m^3 in comparison to 1.7 to 3.7 mW/m^3 under the cratons (Majorowicz and Grasby, 2010a).

5. **Geothermal heat flow**: The geothermal gradient in the Rocky Mountains is higher than in adjacent cratons, leading to increased heat flow. This could be attributed to elevated temperatures in the mantle under the Rocky Mountains relative to the stable craton areas (Figure 25). The estimated temperatures at the Moho for most of the Cordillera is between 800 °C and 850 °C compared to 400 °C and 450 °C in craton areas (Lewis *et al.,* 2003; Hyndman, 2017).

6. **Lithosphere delamination:** lithospheric delamination can influence the depth of the Curie isotherm in several ways (Bao *et al*., 2014):

- **Increases heat flow**: When the dense lithosphere detaches it increases heat flow from rising asthenospheric material.

- **Thinning of the lithosphere**: Delamination results in a thinner lithosphere, which reduces the distance between the surface and the heat-producing mantle. This contributes to elevated temperatures at shallower depths.

- **Localized magmatism**: The upwelling of asthenospheric material can cause partial melting, leading to magmatic activity. This further enhances heat flow and affects the thermal structure of the region.

The depth to Moho, determined through 3D gravity inversion in this study, varies between 35.0 km and 45.6 km, with an average depth of 38.3 ± 2.2 km. Regionally, the Moho is shallower in northeastern Alberta (~ 35 km), and deeper (~ 45 km) in the southwestern Alberta. Interestingly, these Moho depth trends contrast with the observed CPD across Alberta. Although positive correlations between Moho and CPD depths have been reported in certain regions, recent studies, such as Chun-Feng Li *et al*. (2019), suggest that CPD depths are independent of Moho depths. This is due to the distinct nature of these boundaries: the Moho represents a lithological boundary, while the CPD reflects a thermal boundary.

However, most of the North American Cordillera, in which the Rocky Mountains represent its easternmost part, is considered to have a relatively thin crust (For example, Hyndman and Currie, 2011) despite its high elevations, which is often attributed to the hot backarc environment and thermal expansion, rather than a thickened crustal root. Thus, most of the Cordillera region has undergone significant crustal extension, leading to a thin lithosphere and high heat flow, much like the Basin and Range Province in western USA.

REFERENCES

Alberta Energy (2021). Renewing Alberta's mineral future: a strategy to re-energize Alberta's mineral sector. Ministry of Energy, Government of Alberta. https://open.alberta.ca/publications/renewing-albertas-mineral-future.

Alberta Geological Survey (2024). High quality regional airborne geophysical surveys in Alberta, version 3, Alberta Energy Regulator.

Alberta Geological Survey (2025). Alberta Geological Survey website. https://ags.aer.ca/research-initiatives/mineral-mapping-program.

Bachu, S., Burwash, R.A (1994). Geothermal Regime in the Western Canada Sedimentary Basin. In G. D. Mossop and I. Shetsen (Comp.). Geological Atlas of the Western Canada Sedimentary Basin. Canadian Society of Petroleum Geologists and Alberta Research Council.

Bansal, A. R., Gabriel, G., Dimri V. P., and Krawczyk, C. M. (2011). Estimation of depth to the bottom of magnetic sources by a modified centroid method for fractal distribution of sources: An application to aeromagnetic data in Germany, Geophysics 76, 11-22.

Bao, X., Eaton, D. W., & Guest, B. (2014). Plateau uplift in western Canada caused by lithospheric delamination along a craton edge. Nature Geoscience, *7*(11), 830–833.

Bhattacharyya, B.K. and Leu, L.K. (1975). Spectral Analysis of gravity and magnetic anomalies due to two dimensional structures. Geophysics, 40, 993-1013.

Bhattacharyya, B.K. and Leu, L.K. (1977). Spectral analysis of gravity and magnetic anomalies due to rectangular prismatic bodies. Geophysics, 41, 41-50.

Blakely, R. J. (1988). Curie temperature isotherm analysis and tectonic implications of aeromagnetic data from Nevada. Journal of Geophysical Research, 93 (B10), 11,817–11,832

Blakely, R.J. (1996). Potential Theory in Gravity and Magnetic Applications. Cambridge Univ. Press

Bouligand, C., Jonathan, M., Glen, G. and Blakely, J.R. (2009). Mapping Curie temperature depth in the western United States with a fractal model for crustal magnetization. Journal of Geophysical Research, 114, 1-25.

Burwash, R.A. and Power, M.A. (1991). Trout Mountain anomaly, northern Alberta: its role in the northwest foreland of the Trans-Hudson orogeny. In The Early Proterozoic Trans-Hudson Orogen of North America. J.F. Lewry and M.R. Stauffer (editors). Geological Survey of Canada, Special Paper 37, 301-311.

Fedi, M., Quarta, T. and De Santis, A. (1997). Improvements to the Spector and Grant method of source depth estimation using the power law decay of magnetic field power spectra. Geophysics. 62, 1143-1150.

Gomez-Ortiz, D. (2005). 3DINVER.M: a MATLAB program to invert the gravity anomaly over a 3D horizontal density interface by Parker-Oldenburg's algorithm. Computers and Geoscience 31, 513-520.

Gaudreau, É. Audet, P. and Schneider, D. A. (2019). Mapping Curie depth across western Canada from a wavelet analysis of magnetic anomaly data. Journal of Geophysical Research: Solid Earth, 124(5), 4365–4385.

Hassan, H. H., Harms, P., (2024a). Geothermal potential of southeastern Alberta, Canada using potential field geophysical data, Proceedings GeoConvention 2024; Calgary, Canada, June 17-19 2024.

Hassan, H. H., Harms, P. (2024b). Radiogenic heat production (RHP) over an area in SE Alberta calculated from radioactive elements ^{238}U, ^{232}Th and ^{40}K detected from airborne gamma-ray spectrometry survey, Proceedings GeoConvention 2024; Calgary, Canada, June 17-19 2024

Hyndman, R.D. (2010). The consequences of Canadian Cordillera thermal regime in recent tectonics and elevation: a review. Canadian Journal of Earth Sciences, V.47, 621-632.

Hyndman, R.D. (2017). Lower-crustal flow and detachment in the North American Cordillera: a consequence of Cordillera-wide high temperatures. Geophysical Journal International, 209, 1779–1799

Hyndman, R.D. (2023). The thermal regime of NW Canada and Alaska, and tectonic and seismicity consequences. Geochemistry, Geophysics, Geosystems, 24

Hyndman, R. D., & Currie, C. A. (2011). Why is the North America Cordillera high? Hot backarcs, thermal isostasy, and mountain belts. Geology, 39(8), 783–786.

Hyndman, R. D., Currie, C. A., Mazzotti, S., & Frederiksen, A. (2009). Temperature control of continental lithosphere elastic thickness, Te vs Vs. Earth and Planetary Science Letters, 277(3–4), 539–548.

Hyndman, R.D. and Lewis, T.J. (1999). Geophysical consequences of the Cordillera–Craton thermal transition in southwestern Canada. Tectonophysics, 306, issue 3-4, 397-422.

Jessop, A. M. (1998). Geothermal energy in Canada. Journal Geoscience Canada, 25, 1, 33–41.

Kaban, M. K. and Mooney, W. D. (2001). Density structure of the lithosphere in the southwestern United States and its tectonic significance. Journal of Research, 106, 721–739.

Lewis, T. J., Hyndman, R.D., Fluck, P. (2003). Heat flow, heat generation, and crustal temperatures in the northern Canadian Cordillera: Thermal control of tectonics. Journal of Geophysical Research, 108, no. B6. 2316, 16-1 to 16-18.

Li, C. F., Lu, Y. and Wang, J. (2017). A global reference model of Curie-point depths based on EMAG2. Nature Scientific Reports, 7, 45129.

Li, C. F., Shi, X., Zhou, Z., Li, J., Geng, J. and Chen, B. (2010). Depths to the magnetic layer bottom in the South China Sea area and their tectonic implications. Geophysical Journal International, 182(3), 1229–1247.

Li, C. F., Wang, J., Lin, J. & Wang, T. (2013). Thermal evolution of the North Atlantic lithosphere: new constraints from magnetic anomaly inversion with a fractal magnetization model. Geochemistry, Geophysics, Geosystems, 14 (12), 5078–5105.

Li, C-F, Zhou, Duo, and Wang, Jian (2019). On application of fractal magnetization in Curie depth estimation from magnetic anomalies. Acta Geophysica, 67, 5, 1319-1327.

Lucazeau, F. (2019). Analysis and mapping of an updated terrestrial heat flow data set. Geochemistry, Geophysics, Geosystems, 20, 4001–4024.

Majorowicz, J. A. (2018). Heat flow–heat production relationship not found: What drives heat flow variability of the Western Canadian foreland basin? International Journal of Earth Sciences, 107(1), 5–18.

Majorowicz, J., Chan, J., Crowell, J., Gosnold W., Heaman, LM„ Kück, J., Nieuwenhuis. G., Schmitt, D.R., Unsworth, M.J., Walsh, N., Weides, S. (2014): The first deep heat flow determination in crystalline basement rocks beneath the Western Canadian Sedimentary Basin, Geophysical Journal International, 1-17.

Majorowicz, J.A. and Grasby, S.E. (2010a). Heat flow, depth–temperature variations and stored thermal energy for enhanced geothermal systems in Canada. Journal of Geophysics and Engineering. 7, 232–241.

Majorowicz, J., Grasby, S.E. (2010b). High potential regions for enhanced geothermal systems in Canada. Natural Resources Research 19, 177–188.

Majorowicz, J. and Weides, S. (2013): Geothermal plays in deep foreland basins of the Canadian Cordillera, Canada GRC Review Canadian Geothermal Research Council, 5, (2013), 2-5.

Mandelbrot, B. B. (1983). The fractal geometry of nature, W. H. Freeman, San Francisco.

Maus, S. and Dimri, V.P. (1994). Scaling properties of potential fields due to scaling sources. Geophysical Research Letters, 21(10), 891–894

Maus, S., Gordon, D. and Fairhead, D. (1997). Curie temperature depth estimation using a self-similar magnetization model, Geophysical Journal International, 129, 163-168.

McCafferty, A.E., Bankey, Viki, and Brenner, K.C. (1998). Montana aeromagnetic and gravity maps and data. U.S. Geological Survey Open-File Report 98–333, URL: http://pubs.usgs.gov/of/1998/ofr-98-0333/mt.html.

Natural Resources Canada (2025a). Canada - Aeromagnetic survey data compilation. https://open.canada.ca/data/en/dataset/

Natural Resources Canada (2025b). Canada - Gravity data compilation. https://open.canada.ca/data/en/dataset/

Okubo, Y., Graf, R.J., Hansen, R.O., Ogawa, K. and Tsu, H. (1985). Curie point depths of the island of Kyushu and surrounding areas Japan. Geophysics, 53, 481-494

Oldenburg, D.W. (1974). The inversion and interpretation of gravity anomalies. Geophysics, 39, 4, 526-536.

Parker, R. L. (1973). The Rapid Calculation of potential anomalies. Geophysical Journal of the Royal Astronomical Society, 31, 447-455.

Pilkington, M., Gregotski, M. E., and Todoeschuck, J. P. (1994). Using fractal crustal magnetization models in magnetic interpretation. Geophysical Prospecting, 42, 6, 677–692.

Pilkington, M., Miles, W., Ross, G.M. and Roest, W. (2000). Potential field signatures of buried Precambrian basement in the Western Canada Sedimentary Basin, Canadian Journal of Earth Sciences*.,* 37, 11, 1453–1471.

Pilkington, M. and Todoeschuck, J. P. (1993). Fractal magnetization of continental crust. Geophysical Research Letters, 20, 627-630.

Porter, W.J., Raymond, A. P., and McCrossan, R.G. (1982). The Western Canada Sedimentary Basin. Philosophical Transactions of the Royal Society of London. A305.169-192

Ravat, D., Pignatelli, A., Nicolosi, I. and Chiappini, M. (2007). A study of spectral methods of estimating the depth to the bottom of magnetic sources from near-surface magnetic anomaly data. Geophysical Journal International, 169, 421-434.

Ross, G.M., Broome, J. and Miles, W. (1994): Potential fields and basement structure – Western Canada Sedimentary Basin; Chapter 4 in Geological History of the Western Canada Sedimentary Basin, G. D. Mossop and I. Shetsen (Comp.), Canadian Society of Petroleum Geologists and Alberta Research Council, Calgary, Alberta.

Salem, A., Green, C., Ravat, D., Singh, K.H., East, P., Fairhead, J.D., Mogren, S. and Biegert, E. (2014). Depth to Curie temperature across the central Red Sea from magnetic data using the de fractal method. Tectonophysics, 75-86.

Spector, A. and Grant, F.S. (1970). Statistical models for interpreting aeromagnetic data. Geophysics, 35, 293-302.

Tanaka, A., Okubo, Y. and Matsubayashi, O. (1999). Curie point depth based on spectrum analysis of magnetic anomaly data in East and Southeast Asia. Tectonophysics, 306, 461-470.

Turcotte, D. L., and Schubert, G. (1982). Geodynamics, New York: Wiley, 450p.

Zhou, S., Thybo, H. (1998). Power spectra analysis of aeromagnetic data and KTB susceptibility logs, and their implication for fractal behavior of crustal magnetization. Pure and Applied Geophysics, 151, 147–159.

ATTACHMENTS

Estimating the Curie Point Depth (CPD) isotherm in Alberta using aeromagnetic data

March 24, 2025

Attached are the results of computing CPD over Alberta. The grids are in Geosoft format.

MERGED_gravity_magnetic_data

MERGED_BOUGUER_2km_TM10CM115_N83.grd → Merged Bouguer Gravity Grid

MERGED_RMI_200m_TM10CM115_N83.grd → Merged RMI magnetic grid

MOHO-from_3D_gravity_inversion

Depth_Moho.grd → Depth to Moho grid

Observed_Bouguer_gravity.grd → Observed gravity (input data)

Bouguer_Calculated.grd → Calculated Bouguer gravity by forward modelling

Diff_Obs-Cal_gravity.grd → Difference between observed gravity and model gravity (i.e. error)

RESULTS_Centroid_method

CPD_centroid_method.grd → Depth to Curie point depth using centroid method

Geothermal_gradient_centroid_method.grd → Geothermal gradient using centroid method

Heat_flow_Centroid_method.grd → Heat flow using centroid method

CPD_Centroid_method.xlsx → Excel sheet of results of centroid method

RESULTS_Fractal_method

CPD_Fractal_method.grd → Depth to Curie point depth using fractal method

Geothermal_gradient_Fractal_method.grd → Geothermal gradient using fractal method

Heat_flow_Fractal_method.grd → Heat flow using fractal method

CPD_Fractal_method.xlsx → Excel sheet of results of fractal method

---

DATA PROJECTION

Projection: Alberta 10 TM

Datum: NAD83 (WGS84)

Central Meridian: 115 West

False Easting: 500000 meters

False Northing: 0 meters

Scale Factor: 0.9992
